Biochimica et Biophysica Acta 1837 (2014) 1047–1062

Contents lists available at ScienceDirect

Biochimica et Biophysica Acta

journal homepage: www.elsevier.com/locate/bbabio

Review

Functional and structural dynamics of NhaA, a prototype for Na^+ and H^+ antiporters, which are responsible for Na^+ and H^+ homeostasis in cells ☆

Etana Padan

Biochemistry, Institute of Life Sciences, Hebrew University of Jerusalem, 91904 Jerusalem, Israel

ARTICLE INFO

Article history:
Received 17 September 2013
Received in revised form 9 December 2013
Accepted 13 December 2013
Available online 19 December 2013

Keywords:
Membrane protein
Membrane transport
Secondary transporter
Antiporter
pH regulation
Bioenergetics

ABSTRACT

The crystal structure of down-regulated NhaA crystallized at acidic pH 4 [21] has provided the first structural insights into the antiport mechanism and pH regulation of a Na^+/H^+ antiporter [22]. On the basis of the NhaA crystal structure [21] and experimental data (reviewed in [2,22,38] we have suggested that NhaA is organized into two functional regions: (i) a cluster of amino acids responsible for pH regulation (ii) a catalytic region at the middle of the TM IV/XI assembly, with its unique antiparallel unfolded regions that cross each other forming a delicate electrostatic balance in the middle of the membrane. This unique structure contributes to the cation binding site and allows the rapid conformational changes expected for NhaA. Extended chains interrupting helices appear now a common feature for ion binding in transporters. However the NhaA fold is unique and shared by ASBTNM [30] and NapA [29]. Computation [13], electrophysiology [69] combined with biochemistry [33,47] have provided intriguing models for the mechanism of NhaA. However, the conformational changes and the residues involved have not yet been fully identified. Another issue which is still enigma is how energy is transduced "in this 'nano-machine.'" We expect that an integrative approach will reveal the residues that are crucial for NhaA activity and regulation, as well as elucidate the pHand ligand-induced conformational changes and their dynamics. Ultimately, integrative results will shed light on the mechanism of activity and pH regulation of NhaA, a prototype of the CPA2 family of transporters. This article is part of a Special Issue entitled: 18th European Bioenergetic Conference.

© 2014 Elsevier B.V. All rights reserved.

1. Introduction

Na^+ and H^+ are among the most prevalent ions in living cells and are essential in cell bioenergetics. An appropriate concentration of these ions within the cell is crucial for the functioning of proteins, whereas an overly high or low concentration of either ion is a powerful stressor to the cell [1]. Thus, all living cells are critically dependent on homeostatic mechanisms that regulate intracellular pH, Na^+ content, and, correspondingly, cell volume [2].

Na^+/H^+ antiporters are actively involved in these homeostatic mechanisms (see [2,3] for recent reviews). In 1974, P. Mitchell and colleagues [4] discovered sodium proton antiport activity in bacterial cells and suggested that Na^+/H^+ antiporter proteins have primary roles in the homeostasis of these cations. Over the 40 years since, sodium proton antiporters have been identified in the cytoplasmic and organelle membranes of almost all cells, including those of plants, animals and microorganisms [5,6], with the exception of one bacterium [7]; furthermore, these antiporters have long been human drug targets [8].

The genome project has yielded a multiplicity of genes that encode putative Na^+/H^+ antiporters; these antiporters have been classified into families on the basis of evolutionary origin. Sodium proton antiporters are members of the monovalent cation proton antiporter (CPA) superfamily (http://www.tcdb.org/). Two subfamilies, NHE [9] and NHA [10], contain orthologues ranging from bacterial to human, and possibly share a similar structural fold [10–13].

EcNhaA (hereafter referred to as NhaA, unless otherwise stated), is the principal Na^+/H^+ antiporter in *Escherichia coli* and is indispensable for the bacterium's adaptation to high salinity, for challenging Li^+ toxicity, and for growth at alkaline pH (in the presence of Na^+ [14]). NhaA is highly prevalent in enterobacteria [15] and has orthologues throughout the biological kingdoms, including in humans [10]. Recently, a homologue of NhaA has been shown to be essential for *Yersinia pestis* virulence and is therefore a novel drug target [16].

Several biochemical characteristics of NhaA underpin its physiological roles: very high turnover [17], electrogenicity with a stoichiometry of $2H^+/Na^+$ [18], and strong pH dependence [17], a property it shares with other prokaryotic antiporters [14] as well as eukaryotic Na^+/H^+ antiporters [6,9,19,20].

2. Structural insights associated with the NhaA crystal structure

2.1. Down-regulated NhaA in acidic pH

The crystal structure of down-regulated NhaA, crystallized at acidic pH 4 ([21] and Figs. 1a and 2c), has provided the first structural insights

☆ This article is part of a Special Issue entitled: 18th European Bioenergetic Conference.

0005-2728/$ – see front matter © 2014 Elsevier B.V. All rights reserved.
http://dx.doi.org/10.1016/j.bbabio.2013.12.007

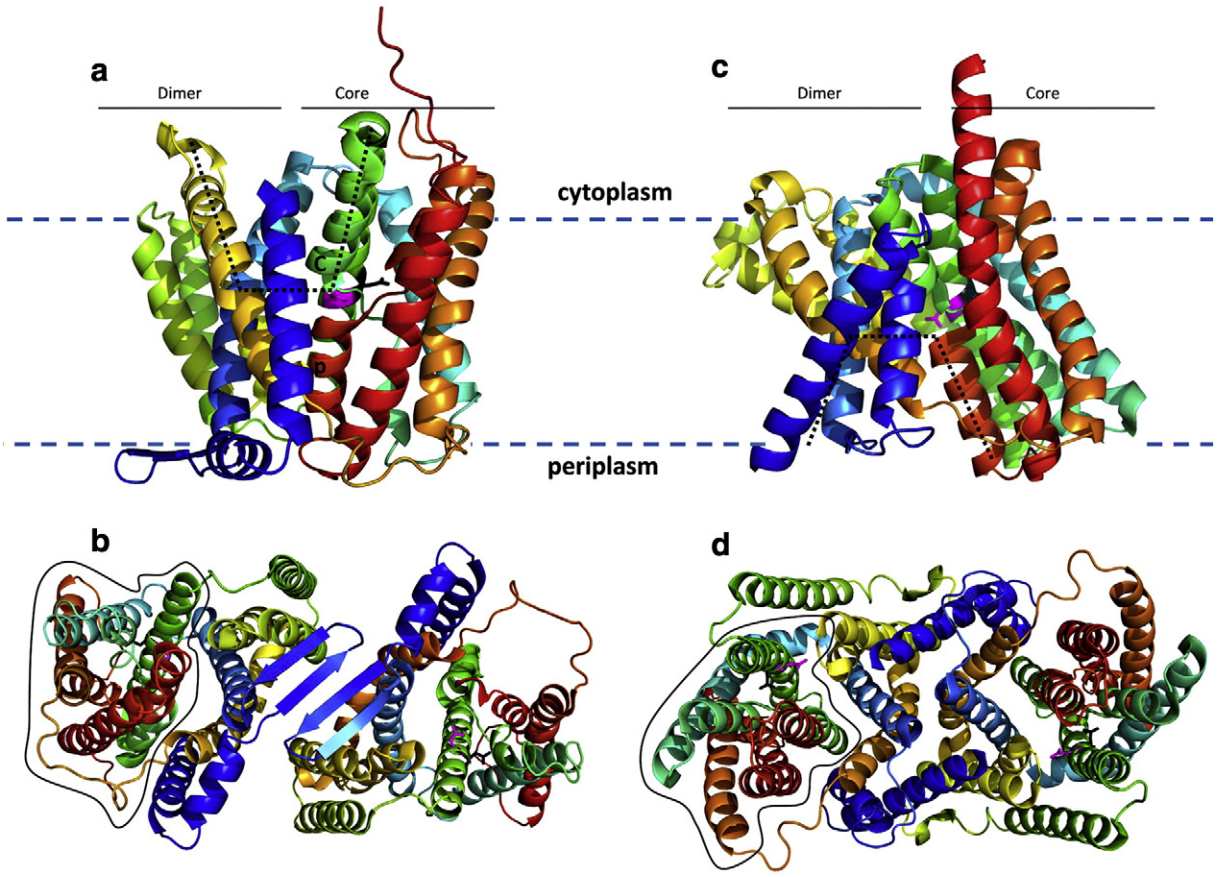

Fig. 1. General architecture of NhaA and NapA. NhaA from *Escherichia coli* [21], $ASBT_{NM}$ from *Neisseria meningitidis* [30] and NapA from *Thermus thermophilus* [29] share a common fold referred to as the NhaA fold (Fig. 2 [37]). (a) Ribbon representation of the crystal structure of NhaA [21] viewed parallel to the membrane (broken light blue line). The 12 TMs are rainbow colored from the N-terminus (blue) to the C-terminus (red). The cytoplasmic funnel is marked (black dotted line). Cytoplasmic- and periplasmic-oriented TMs of the TMs assembly are denoted c and p, respectively. Asp163 and Asp164 are colored black and magenta respectively. The dimer interface and core are underlined. (b) The NhaA dimer viewed from the periplasm. The core domain is encircled on the left protomer. (c) Ribbon representation of NapA [29]. The 13 helices are rainbow colored from N-terminus (blue) to C-terminus (red). Asp156 and Asp157 are colored black and magenta respectively. The dimer interface and core are underlined. (d) The NapA dimer viewed from the periplasm.

into the antiport mechanism and pH regulation of an Na^+/H^+ antiporter [22]. NhaA consists of 12 transmembrane helices (denoted "TMs"; N and C-termini on the cytoplasmic side of the membrane) organized in a novel fold comprising two topology-inverted repeats. The first structural repeat includes TMs III, IV, V and TMs X, XI, XII [21]. The second structural repeat includes TMs I, II and VIII, IX [13]. In the first NhaA repeat, one TM (IV or XI) is interrupted by an extended chain in the middle of the membrane, connecting two short helices (IVc and IVp, or XIc and XIp, respectively) oriented to the cytoplasm (c) or periplasm (p) [21]. This non-canonical assembly, denoted TM IV/XI, creates a delicately balanced electrostatic environment in the middle of the membrane at the ion-binding site(s), suggesting that the assembly has a critical role in the cation exchange activity of the antiporter [21].

Another crystal structure of NhaA has recently been determined at pH 3.5 at a resolution of 3.5 Å (PDB IDs: 4AU5, 4ATV; preliminary results of Cameron, A., and Drew, D.). Both this structure and the structure determined in [21] were obtained at acidic pH, suggesting that acidic pH is energetically favorable for NhaA crystallization. Satisfactorily, the two structures are identical aside from loops and the position of TM X (Fig. 3a and b). In the first determined structure, helix X had the highest B factor in the structure, implying instability [21]. The medium resolution of this structure and the high B factor of helix X may have led to a mistaken assignment. However, because of the high B factor it is also possible that the two structures show two different conformations of NhaA. Notably, a pH-induced movement of helix X has been observed experimentally [23].

Similar to many secondary transporters, NhaA is a dimer. Several experimental approaches have strongly suggested that NhaA is a dimer in the native membrane; genetic complementation [24], biochemical pull-down experiments [24], intermolecular cross-linking [24], ESR studies [25,26] and cryo-electron microscopy of 2D crystals [27,28]. Recently, the 3D crystal structure of the NhaA dimer has been determined (PDB IDs: 4AU5, 4ATV; preliminary results of Cameron, A., and Drew, D. and Fig. 3b). The NhaA dimer interface is formed by a β-sheet at the periplasmic side and few contacts between TMs IX and VII at the cytoplasmic side (see below, Sections 2.2.1 and 3.1.4).

2.2. NapA and ASBT, antiporters with crystal structures similar to that of NhaA

Two transporters that share the NhaA structural fold have recently been structurally determined: (i) NapA, the Na^+/H^+ antiporter in *Thermus thermophilus* [29], and (ii) a bacterial homologue of the human bile acid transporter ASBT [30]. Insights about the structures of these transporters can shed light on the structure of NhaA, and vice versa.

2.2.1. The crystal structure of NapA

NapA is the Na^+/H^+ antiporter in *Thermus thermophilus* and belongs to the CPA2 clade [31]. It has 21% sequence identity with the human Na^+/H^+ antiporter NHA2 and lower sequence homology to NhaA, <15% sequence identity. NapA, like NhaA, is pH-dependent; it is active above pH 6, with maximum activity for Na^+ at pH 8 [31]. The sensitivity of the exchange rate of NapA to the transmembrane potential ($\Delta\Psi$) suggests that the antiporter is electrogenic, although neither its precise rate nor its stoichiometry has been determined [29]. The crystal structure of

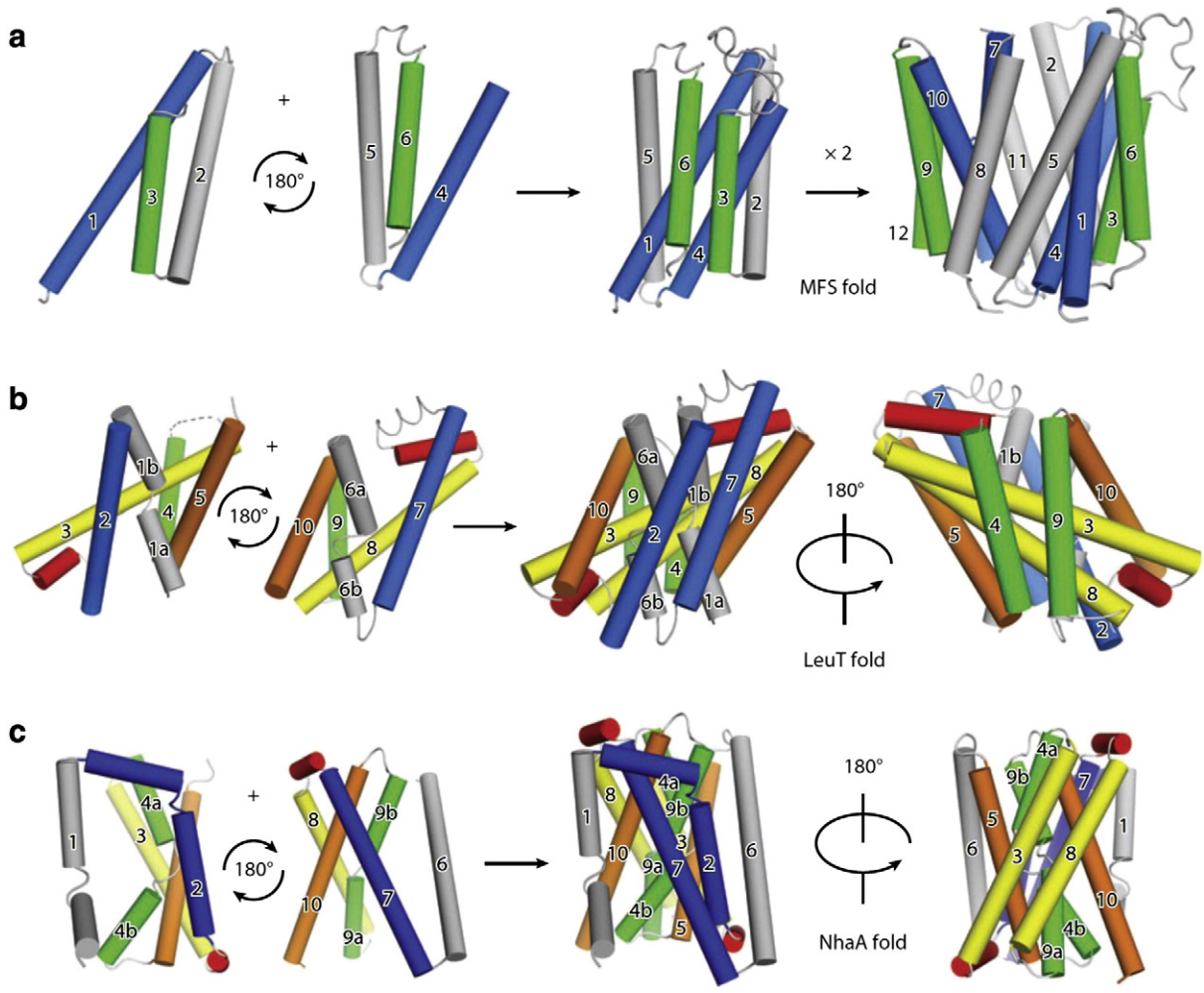

Fig. 2. Three common folds of secondary active transporters. The common folds of secondary transporters according to [37]. (a) The major facilitator superfamily (MFS) fold contains 12 TMs which are organized into N- and C-domains related to each other by a pseudo-twofold symmetry axis that is parallel to the surface normal of the membrane. Each domain comprises two inverted repeats of three consecutive TMs. (b) The LeuT fold comprises 10 TMs that are organized into two inverted structural repeats, each containing 5 consecutive TMs, The first TM in each repeat (TM1 and 6), is discontinuous and consists of two short α-helices connected by highly conserved extended chain. (c) The NhaA fold comprises two inverted structural repeats, each consisting of 5 consecutive TMs. Each repeat contains interrupted helix in TM4 in repeat 1 and TM 11 in repeat 2 in NhaA [21] or TM 9 in $ASBT_{NM}$ [30]. The two pairs of short α-helices in these two TMs cross each other at the center of the structure, using their highly conserved extended chains [21,37].

NapA has recently been determined at a resolution of 3 Å [29] from crystals grown at pH 7.8, when NapA is active.

Each NapA monomer is built of 13 TMs (Fig. 1b) with an N_{out}–C_{in} topology. Relative to NhaA it has an additional helix at the amino terminus. This additional helix is referred to as −1, and the others are 1–12 as in NhaA. There are two topology-inverted repeats, TMs −1,1–5 and 7–12. They intertwine to form a core and a dimerization domain. Overall, the structures of NhaA and NapA are very similar, differing only in the position of the core relative to the dimerization domain. The similarity is best seen when the two domains are superimposed separately (core domain: r.m.s.d. of 1.8 Å; dimerization domain: 1.9 Å). In NapA, the position of the core gives rise to a large negative funnel that is open to the periplasm and is blocked from the cytoplasm. At the bottom of the funnel are two highly conserved aspartates (Asp156, Asp157), which are equivalent to Asp163 and Asp164, located at the bottom of the cytoplasmic funnel of NhaA. Although neither Na^+ nor Li^+ is present in the NhaA and NapA structures [21,29], Asp163 and Asp164 have been identified as the Na^+ binding site of NhaA. This assessment is based on the crystal structure [21], conservation [10] mutants [22,32] and isothermal calorimetry [33]. Mutations obtained in NapA [29,31] and equilibrium molecular dynamics simulations support this conclusion [29,34]. As described below (Section 5.2.1.), determination of the crystal structures of NhaA's inward-open conformation and of NapA's outward-open conformation contributed to the development of a model mechanism for NhaA exchange activity.

Like NhaA, NapA is a dimer but its interface is different. In NhaA, the main contact is formed by a β-sheet at the periplasmic side ([21,26,35] and Fig. 1b) and only few contacts between TMs IX (Trp258) and VII (and also possible a contact betweenVal254 and Arg204) at the cytoplasmic side. Most likely, lipids fill the space between the protomers. The β-sheet is responsible for the NhaA dimer stability because deletion of the β-sheet produces a monomeric NhaA (see Section 3.1.4). In marked contrast, NapA lacks the β-hairpin and the dimer interface is formed by tight helices contacts within the membrane (mainly between TM −1 on one monomer and TM 7 on the other and some contacts between the ends of TM 2 and TM 9 [29] and Fig. 1d). The dimer interface of NapA more closely resembles the dimer interface modeled in the 7 Å electron crystallography structure of NhaP1, a CPA1 member from *Methanocaldococcus janaschii* which also has 13 helices [36].

2.2.2. The crystal structure of $ASBT_{NM}$

The crystal structure of $ASBT_{NM}$, a bacterial homologue from *Neisseria meningitidis* of the human bile acid transporter ASBT, was determined at a resolution of 2.2 Å [30]. Overall, the architecture of this protein shows a fold very similar to that of NhaA (Fig. 2c), despite having no detectable sequence homology. In $ASBT_{NM}$, as expected for

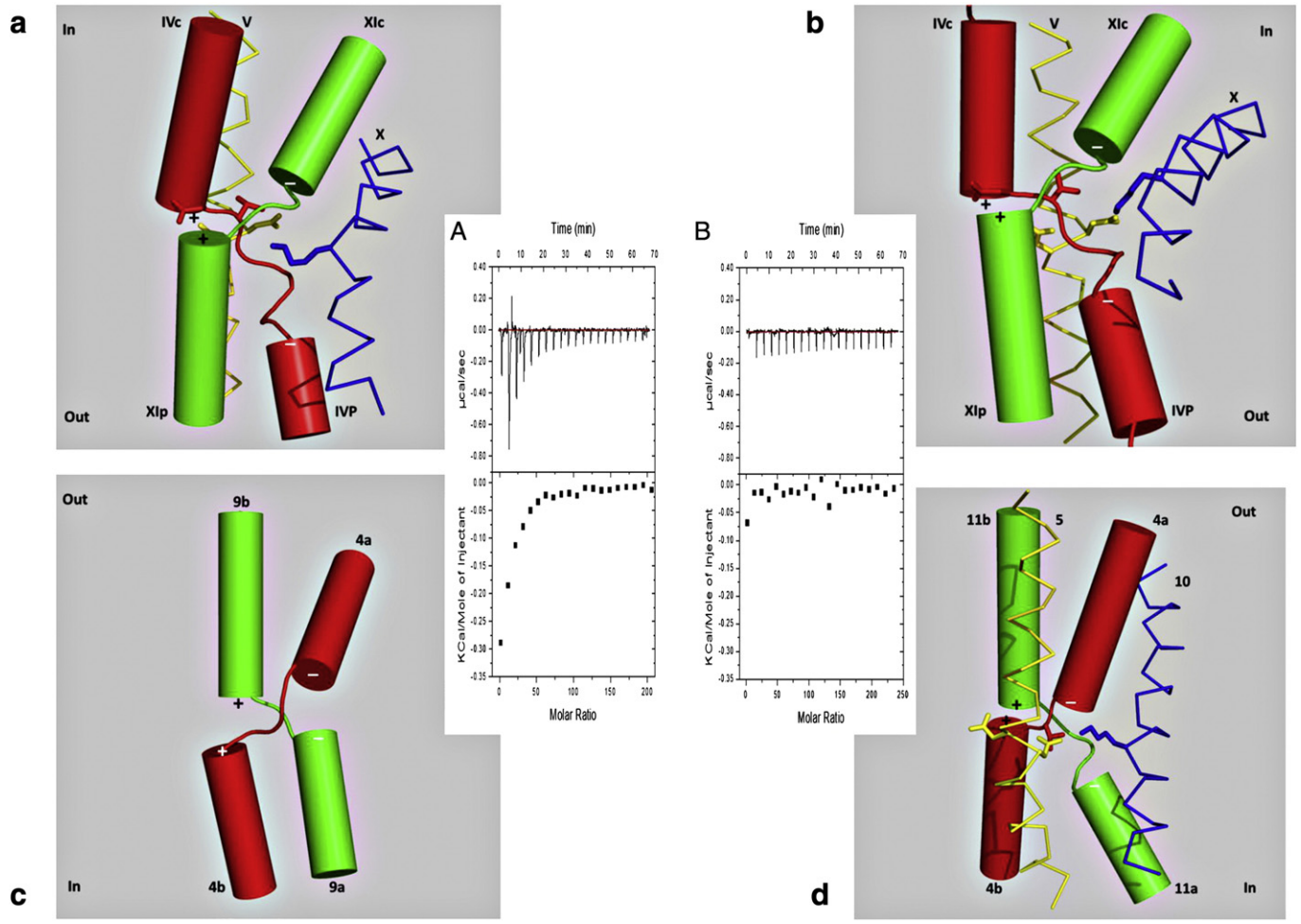

Fig. 3. The binding sites at the interrupted helices that cross each other in the NhaA fold members. (a) The Na^+ binding site identified in the original NhaA structure is shown at the crossing of the interrupted helices (TM IV/IX assembly) [21]. (b) The Na^+ binding site identified in the new NhaA structure is shown at the crossing of the TM IV/XI assembly. (c) Crossing of the interrupted helices in $ASBT_{NM}$ [30]. (d) The putative Na^+ binding site of NapA [29]. In the middle, isothermal titration calorimetry (ITC) shows that NhaA specifically binds Li^+ (A) but does not bind K^+ (B). Titrations of 40 mM LiCl into 50 µM wild-type NhaA protein or of 40 mM KCl into 35 µM wild-type NhaA protein were done in steps of 2 µl every 200 s in a reaction mixture containing 50 mM BTP (1,3-bis-[tris(hydroxyl methyl)methylamino]propane), 150 mM choline chloride, 5 mM MgCl2, 10% sucrose and 0.015% n-dodecyl—β-D-maltoside. This assay revealed the thermodynamics of Li^+ binding to NhaA (see Section 3.1.2 and [33]).

proteins with an NhaA fold, the interrupted helices cross each other in proximity to the identified sodium-binding site [30] (Fig. 3c). This characteristic of the NhaA fold served as a basis for prediction of the Na^+ binding site of NhaA; predictions are in line with previous suggestions based on indirect evidence (Section 3.1.2 and Figs. 1 and 3).

2.3. The NhaA fold

As shown above with the crystal structures of NhaA, NapA and ASBT, there are other multiple types of membrane transporters that share no apparent sequence similarity yet share a common structural fold [37]. At least three such common folds have been identified among the secondary transporters (Fig. 2): the MFS fold, the LeuT fold, and the NhaA fold [37]. Remarkably, like the NhaA fold, many of the structural folds of secondary transporters include inverted topological repeats containing interrupted helices (discontinuous, unwound helices) with functional implications similar to those of NhaA, discussed in further detail below (reviewed in [37–41]).

2.3.1. Discontinuous helices

Two types of discontinuous helices have been observed in transport proteins: transmembrane-spanning and hairpin-type [42]. The transmembrane-spanning class is present in NhaA and in LeuT, a neurotransmitter transporter bacterial homologue from *Aquifex aeolicus* [43]. In both NhaA and LeuT, transmembrane-spanning discontinuous helices appear in pairs, where each member of a given pair is part of an inverted repeat. The members of a helix pair may be positioned either in parallel to each other (as in LeuT [43]) or crossing over each other (as in NhaA [21], ASBT [30]) and NapA [29]. The hairpin-type class is present, for example, in the chloride/H^+ exchanger (CLC, [44]) and in the glutamate transporter bacterial homologue from *Pyrococcus horikoshii* (Glt_{ph}) [45]. The term "hairpin" refers to the placement of the unwound segment (extended chain), connecting two antiparallel half-helices within the membrane.

Importantly, extended chains in the middle of the membrane have been shown to play an indispensable role in ion transport. They participate in the ion-binding sites of many of the transporters whose crystal structures have been determined since that of NhaA [30,42]. Unlike in a helix, in an extended chain the main-chain oxygen and amide are not fully saturated with internal hydrogen bonds. Therefore, an extended chain can supply main-chain carbonyl oxygen and amide to coordinate Na^+ together with charged and polar side-chains from surrounding amino acids [42]. The dipole moment of the connecting helices' termini also contributes to the coordination of ions or substrate molecules [42]. In addition to coordinating ions, the extended chains, which are flexible, create a defined open niche for accommodation of a charged substrate in an otherwise densely packed environment, typical for α-helical integral membrane proteins. Furthermore, transport processes are

associated with conformational changes. Extended chains participate in these changes, conferring flexibility at lower energetic cost compared with α-helices (Section 4.3.2).

Although extended chains interrupting helices in the middle of the membrane have since been recognized as a common feature for ion binding in transporters [42], the antiparallel crossing over of the TMs is a unique feature of the NhaA fold. It results in the positive dipole ends of TM IVc and TM XIp facing one another and likewise the negative dipole ends of TM IVp and XIc (Fig. 3). In NhaA the dipoles are proposed to be neutralized, respectively, by the side-chains of Asp133 and Lys300 [21]. NapA features Lys305, equivalent to Lys300 in NhaA, but instead of Asp133, it contains Ser, as does human NHA2 [46]. It is possible that Glut333 compensates for the positive charge associated with this difference. In addition to charge compensation, Asp133 changes conformation with pH [47], and Lys300 plays a major role in pH regulation of NhaA [33].

2.4. Evolution-based computational modeling of prokaryotic and eukaryotic Na^+/H^+ antiporter structures

Membrane proteins make up about 60% of drug targets, and about 20% of these membrane proteins are transporters. As yet, very few structures of eukaryotic transporters have been determined [48,49]. Nevertheless, prokaryotic transporters, which are much easier to express compared with eukaryotic transporters, have proved to be very good models of drug targets. This is mainly a result of homology modeling techniques that have provided structural knowledge about membrane proteins and their interactions with drugs and other molecules. For example, a bacterial homologue of the human monoamine neurotransmitter transporter *Aquifex aeolicus* ($LeuT_{Aa}$) [39,43] has been used as a model of the neurotransmitter sodium symporters (NSS), molecular targets of many pharmacologically active substances. Homology models of NSS proteins, combined with site-directed mutagenesis data, have identified ligand-binding sites and contributed important insights towards new drug development.

2.4.1. Eukaryotic transporters

Using the crystal structure of NhaA as a template, along with evolutionary conservation data, a range of computational tools have been developed and used to predict the 3D structures of human NHE1 and NHA2 [11,46]. These Na^+/H^+ exchangers are vital for cellular homeostasis and play key roles in pathological conditions such as cancer and heart diseases (NHE1) [8] and essential hypertension (NHA2) [50,51]. Modeling these structures was particularly challenging because of their extremely low sequence identity with NhaA. Yet, NHE1 and NHA2 each has a distant evolutionary relationship with NhaA, which enabled evolutionary conservation analysis to be used in the modeling.

The 3D model obtained for NHE1 [11,46] was supported by evolutionary conservation analysis and empirical data. It also revealed the location of the binding site of NHE inhibitors; Mutations that alter the binding affinity of the NHE inhibitors were located in equivalent positions in a few eukaryotic NHE isoforms, implying that these isoforms share a common binding site [11]. This prediction was validated by conducting mutagenesis studies with EcNhaA and its specific inhibitor 2-aminoperimidine [52]. Asn64, Phe71 and His225 in NhaA were found to contribute to the AP binding site [11]. The model-structure features a cluster of titratable residues that are evolutionarily conserved and are located in a conserved region in the center of the membrane, implying that they are involved in cation binding and translocation.

The Landau model presents a novel topology. A previously suggested topology was based on hydrophobicity scale and assessed by accessibility test of Cys replacements along the molecule from either side of the membrane [53]. This work yielded conflicting results in several regions. Whereas, the irst TM in Landau model begins at Val129, the other topology model predicted two additional segments at the N-terminal end. In support of Landau model this segment is not conserved and chymotryptic cleavage of the NHE1 N-terminal region (residues 1–150) indeed had little effect on the transport activity [54]. Recently, another human NHE1 model structure, based on NhaA crystal structure was suggested [55]. The model was supported by a single electron paramagnetic resonance measurement. This single data was found equally compatible with both structure models and does not substantiate either of them. Overall, incorporating structural and experimental information, we suggest that the Landau model better captures the essence of the functional elements of NHE1 and depicts a more reliable structural scaffold [56]. For further discussion see [57].

Human NHA2 is a poorly characterized Na^+/H^+ antiporter that has only recently been implicated in essential hypertension [58]. The computationally derived model structure, based on the crystal structure of NhaA, guided mutagenic evaluation (based on phenotype screening in yeast) of transport function, ion selectivity, and pH dependence of NHA2. A cluster of essential, highly conserved titratable residues was identified in an assembly region made up of two discontinuous helices of inverted topology, each interrupted by an extended chain. Whereas in NhaA, oppositely charged residues compensate for partial dipoles generated within this assembly, in NHA2, polar but non-charged residues suffice. This study established NHA2 as a prototype for the poorly understood, yet ubiquitous, CPA2 antiporter family recently recognized in plants and metazoans and exemplified a structure-driven approach to obtain functional information on a newly-discovered transporter.

2.4.2. Prokaryotic transporter

Aside from EcNhaA, NhaP1 of *Methanococcus jannaschii* (MjNhaP1) is currently the only other member of the prokaryotic CPA1 superfamily for which structural information is available [59]. Cryo-electron microscopy of 2D crystals has shown that, like EcNhaA, NhaP1 is a dimer, but it differs from EcNhaA in the specific characteristics of its dimer interface. Recently [36], the 3D structure of MjNhaP1 was determined at 7-Å resolution by electron crystallography of 2D crystals. EcNhaA-structure-based modeling of NhaP1 revealed a six-helix bundle core similar in both proteins. This suggests that the motif of unwound regions in two cross-helices is shared by all CPAs. However, NhaP1 has 13 TMs, of which the N-terminal helix is an un-cleaved signal sequence, important for antiporter functionality [36].

3. Functional-organization insights provided by the NhaA crystal structure

Like other secondary transporters, NhaA acts as a "nano-machine". It utilizes energy (proton motive force, PMF, $\Delta\mu_{H+}$) to transfer ions from one side of the membrane to the other by a canonical mechanism: alternate accessibility of the active site to each side of the membrane [60]. Furthermore, NhaA activity is regulated by pH: The antiporter is inactive below pH 6.5, and its rate of activity increases dramatically with pH, achieving its maximum at pH 8.5 [3,17].

What is the functional organization of NhaA? Do amino acid residues involved in the exchange activity of the antiporter overlap with those involved in pH regulation, or do they form separate clusters? The NhaA structure has provided the basis for the rational interpretation of genetic, biochemical, biophysical, structural and computational approaches aimed at gaining insight into the functional organization and dynamics of NhaA. These approaches are reviewed in what follows.

3.1. Structure-based molecular-genetic study of the functional organization of NhaA

Since cloning the NhaA gene [61], we have studied the functionality of NhaA using site-directed and random mutagenesis and developed a highly successful canonical approach, still used today, to select for and characterize interesting mutations in NhaA, as well as in other prokaryotic Na^+/H^+ antiporters. According to this approach, a mutant is transferred on a plasmid to a host that lacks specific Na^+/H^+

antiporters—either NhaA (NM81) [62] or both NhaA and NhaB (EP432) [63] or KNabc and TO114—and that also lacks the non-specific Ca^{++}/H^+ antiporter ChaA [64–66] (review in [38]). These hosts grow on a non-selective medium, LBK (LB of which NaCl is replaced by KCl), but they do not grow on selective media at pH 7 containing high concentrations of Na^+ (0.6 M) or Li^+ (0.1 M) or at pH 8.3 with high concentrations of Na^+ (0.6 M) unless they bear wild-type NhaA or another active Na^+/H^+ antiporter. Therefore, from the growth phenotype, it is possible to deduce the characteristics of a given NhaA variant [67]. Then, to prove the prediction, Na^+/H^+ antiporter activity is determined in isolated membrane vesicles and in proteoliposomes reconstituted with the pure variant protein. Two additional approaches that we have recently introduced for the study of NhaA function are electrophysiology [68,69] and isothermal calorimetry [33] (see Sections 3.1.2 and 5.2.2). In what follows we review these methods in greater detail.

Notably, EP432 has become an important tool not only for identifying mutations in NhaA and other antiporters from *E. coli* but also for selecting suppressor mutations [70] and for cloning and characterizing heterologous antiporter genes [14,67]. This *E. coli* strain has been applied, for example, in the characterization of NapA from *Thermus thermophilus* [31]; NhaD from a plant [71]; and Mrp, the multisubunit antiporter from *Vibrio cholerae* [72], *Staphylococcus aureus*, *Bacillus subtilis* and the alkaliphilic *Bacillus pseudofirmus* OF4 [73].

3.1.1. Site-directed Cys-scanning

Site-directed Cys replacement (Cys-scanning) is an effective experimental approach used preferentially in Cys-less membrane proteins to identify functionally important residues [74–76]. It has proven to be similarly effective when applied to Cys-less NhaA (CL-NhaA), a mutant as active as the wild-type antiporter [77]. In brief, plasmids bearing a single-Cys-replacement variant are transformed into EP432, the *E. coli* strain deleted of *nha*A and *nha*B [63], and the NhaA variant is characterized with the routine protocol described at the beginning of this section (3.1).

We have already Cys-scanned TMs II [78], IV [47], VIII [79], IX [80,81], X [23] and part of XI [82,83] and characterized the mutants. We found new residues that affect the cation translocation and/or pH response. Projecting the mutants' phenotypes onto the structure was enlightening, revealing two functional regions (Fig. 4): (a) a cluster of amino acyl side-chains, involved in pH regulation, is located on TMs IX, IVc, II and loops VIII–IX [22]; this cluster is referred to as the "pH sensor", and (b) a catalytic region containing the ion-binding sites [33] is located on TMs IV, V, X, XI), about 9 Å away from the pH regulation cluster. Notably, the Cys-replacement mutants obtained are useful for many other purposes because the sulfhydryl (SH) of Cys is a reactive residue for site-directed chemical modifications (see Section 4.3).

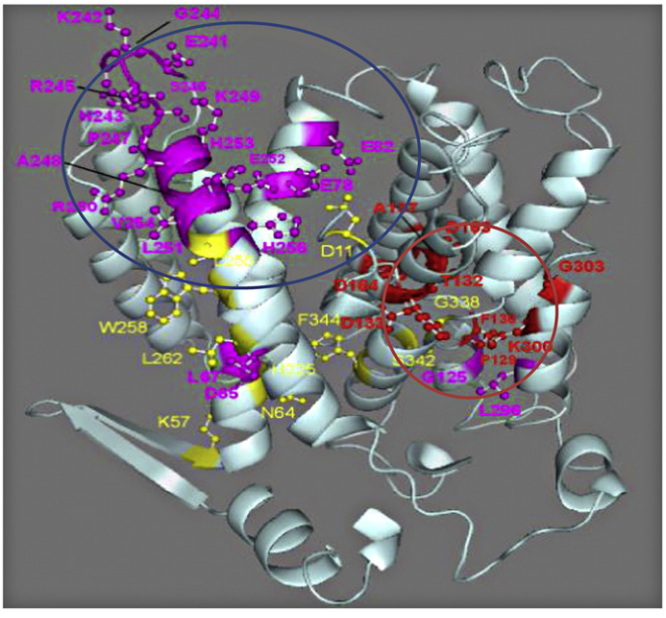

Fig. 4. Functional organization of NhaA. A stick-and-ball representation of functionally important residues in the putative active site (red) and the pH sensor (yellow or magenta) on the NhaA crystal structure.

3.1.2. The active site of NhaA with emphasis on structure and thermodynamics of ion binding

Although neither Na^+ nor Li^+ was observed in the NhaA structure [21], residues Asp163, Asp164 on TM V, Asp133, Thr132 on the extended chain of TM IV and Lys300 on TM X have been suggested to form the NhaA active site. This proposition is based on evolutionary conservation, mutagenesis and location in the NhaA crystal structure (reviewed in [38]). Specifically, these residues are the most conserved [11,23], their mutations either obliterate (D163, D164, [82–85] or impair (T132, D133, and K300) [83,23,33] antiporter activity, and they are clustered at the middle of the TM IV/XI assembly ([21] and Fig. 3). However, because the structure was determined at pH 4.0 (3.45 Å resolution) when NhaA was down-regulated, many questions remain regarding the active conformation(s) at physiological pH, including the conformation of the ligand-active site. Nevertheless, the recently-determined crystal structure of an ASBT homologue, which has an NhaA fold [30], shows the Na^+ binding site exactly at the intersection of the extended chains.

Using isothermal titration calorimetry (ITC) [33], we revealed the thermodynamics of Li^+ binding to NhaA (Fig. 3, middle). The purified NhaA, in detergent micells, binds Li^+ in detergent micelles, and this interaction is driven by an increase in enthalpy (ΔH of -8000 ± 300 cal/mol and ΔS of -15.2 cal/mol/deg at 283 K), involves a single binding site per NhaA molecule and is highly specific. The large negative value of ΔH may suggest tight packing upon ligand binding: a specific conformation of NhaA is selected from the dynamic ensemble of conformations upon ligand binding. Similar binding assays of galactoside-ligands to the H^+/lactose symporter LacY yielded opposite results [86], producing almost no change in ΔH and a remarkable change in $T\Delta S$. It is tempting to suggest that wild-type LacY is more flexible than NhaA and that the thermodynamic difference explains why well-diffracting crystals have been obtained with wild-type NhaA [21], whereas well-diffracting crystals of LacY were first obtained with a mutant C154G, whose thermodynamic characteristics were similar to those of wild-type NhaA [86]. This suggestion is highly speculative, however; water binding and conformational changes may dominate the binding process and affect the thermodynamics results.

As expected given the high pH sensitivity of NhaA (review in [14]), the binding of Li^+ to NhaA in detergent micelles is also very sensitive to pH [33]; ITC signals of Li^+ binding to NhaA were observed only at pH 8.5, the optimal pH of activity in membrane vesicles and liposomes [14,17]. However, the pH sensitivity of Li^+ binding to pure NhaA in detergent micelles was more drastic than in membranes; no ITC signals were observed below or above pH 8.5, while the pH profile in membrane vesicles and liposomes progressively increases between pH 6.5 and 8.5.

The ITC results [33] clearly show that D163 and D164 are part of the cation binding site of NhaA. Their Cys replacements totally abolished Li^+ binding. These two essential and highly conserved aspartate residues are located in the middle of the membrane, very close to the unwound part of the TM IV/XI assembly (Figs. 1 and 3 and [21]), and D164 protrudes into the cytoplasmic funnel, which is open to the cytoplasm [21].

Thr132 and Asp133 form the extended chain that interrupts TM IV in the NhaA TM IV/XI assembly, and Asp133 compensates for the positive charge of the partial dipoles of the interrupted helices (IVc and XIp, Figs. 1a and 3a,b and [21]). As described above (Section 2.3.1), unlike in a helix, in an extended chain the carbonyl oxygen and amide of the

main chain (peptide bond) are not fully saturated with internal hydrogen bonds and can coordinate ions. Hence, two types of residues can be involved in the cation binding site: residues in a helix that coordinate ions via the side-chain, and residues in the extended chain, which may also donate carbonyl or amide of the main chain. Importantly, although both types of residues are involved in the binding site, mutations of the two types may give different phenotypes. In a helix, replacement of a residue that coordinates a ligand via the side-chain usually results in a lethal phenotype, in which case the residue is designated essential. In contrast, in an extended chain, replacement of a residue that coordinates a ligand via the main chain does not necessarily yield a lethal phenotype, because every replacement can provide a peptide bond, and the new side-chains may or may not have indirect effects on the structure and/or function of the protein. For example, Asp163 and Asp164 in helix V are essential; they are irreplaceable, and their variants do not bind ligands. On the other hand, replacement mutants T132C and D133C, in the extended chain, are viable with modified phenotypes, and D133C yields ITC signals of ligand binding [33].

Lys300, a highly conserved residue [23], resides in the vicinity of the C-termini of the interrupted helices, IVp and XIc of the TM IV/XI assembly [21] (Fig. 3a and b) and therefore can compensate for the partial negative charge of the dipoles of their C-termini. The role of the positive charge of K300 was explored using replacements K300H and K300R, potentially positively charged residues assumed to have different pK_a [33]. This assumption was supported by a recent systematic study of Asp, Glu, Lys and Arg residues at 25 internal positions in staphylococcal nuclease [87]. This study showed that whereas the pK_a values of Asp, Glu and Lys can be highly anomalous and shift by as many as 5.7 pH units relative to their pK_a values in water, Arg residues at the same position exhibit no detectable shifts in pK_a and remained charged at pH $\leq$ 10. The unique capacity of Arg side-chains to retain their charge in dehydrated environments probably contributes to the important functional roles of internal Arg in situations in which a charge is needed in the interior of a protein, in a lipid bilayer, or in similarly hydrophobic environments. A comparison of the physiology of K300H and K300R with known acidic or neutral replacements of Lys300 showed that a positive charge at position 300 is essential for NhaA activity, but that there are further subtleties aside from charge *per se* at position 300 that are important for the mechanism of the antiporter.

The mutation K300R caused a dramatic alkaline shift, of one pH unit, in the pH profile of NhaA [33]. Furthermore, the K300R protein in DDM micelles showed small ITC signals only at pH 9.0. We therefore suggest that in the membrane the pK_a of K300 participates in the pH control of NhaA by affecting ligand binding. Because the pK_a of an amino acid in a protein is affected by the surrounding residues, it is likely that the process of purification, which alters this environment, affects the pH sensitivity of the active site in DDM micelles.

In conclusion: Asp163, Asp164, and the backbone of Thr132 and Asp133 (the extended chain) are essential parts of the NhaA cation binding site. The positive charge of Lys300 is essential for antiporter activity, most likely because of its effect on ligand binding. Therefore the pK_a of this residue is an important factor in the pH response of NhaA.

Recently [88], ITC has been used in a very elegant way to measure the H^+/Cl^- stoichiometry of the H^+/Cl^- exchanger. Chloride binding was shown to induce protonation of a crucial Glu. The simultaneous binding of H^+ and Cl^- gives rise to a fully loaded state that is incompatible with the canonical transport mechanism (see above). This suggests that the stoichiometry of transport is determined by the thermodynamics of synergistic substrate binding rather than the kinetics of conformational changes and ion binding.

3.1.3. Random mutagenesis

Mutants that alter ion selectivity and/or energy coupling of a transporter are of special interest for identifying the residues that are most likely to contribute to the ion translocation machinery. Mutants impaired in pH regulation are critical for identifying residues involved in the unique pH response of NhaA. A successful method adopted to select for such NhaA mutants is briefly summarized here. Following PCR-based random mutagenesis, a mutagenized NhaA-encoding plasmid is transformed into KNabc (Δ*nha*AΔ*nha*BΔ*cha*A) [66 [Radchenko, 2006 #308] (see Section 3.1). The transformants are first grown on non-selective medium LBK at pH 7 to form colonies, producing a cell library with mutated plasmidic NhaA. These colonies are then replica-plated on LBK-based selective media with either Na^+ (0.6 M) or Li^+ (0.1 M) at either pH 8.2 or pH 7 to identify various potential NhaA mutants as follows: Mutants that cannot grow on any of the selective media are impaired in antiporter activity; mutants that can grow on only one of the selective media at both pH levels are impaired in ion selectivity; mutants that can grow on the selective media at pH 7 but not at pH 8.2 are impaired in pH response and/or energy coupling. This is because both alkaline pH activation of NhaA [89] and its stoichiometry of $2H^+/Na^+$ (electrogenicity) [2,14] are critical for *E. coli* growth at alkaline pH in the presence of Na^+/Li^+. The electrogenicity enables the membrane potential, the only driving force existing at alkaline pH in *E. coli*, to be exploited [90].

We carried out this process in 60,000 screened cells, of which 10 mutants grew only on the non-selective media, and nine carried more than two mutations in *nha*A, verifying the efficiency of our mutagenesis. One mutant, A167P (Fig. 5a), grew only on selective media at pH 7 on Li^+ (0.1 M) but not on Na^+ (0.6 M). Remarkably, this mutation is located on TM V not far from the putative active site (Fig. 5a), and, most interestingly, and unlike wild-type NhaA, it is indifferent to changes in membrane potential. Wild-type NhaA, like all electrogenic transporters, is highly sensitive to $\Delta\Psi$. This is best observed when ΔpH-driven $^{22}Na^+$ uptake is tested in NhaA proteoliposomes. In the absence of a counter ion the rate of uptake is slow due to the $\Delta\Psi$ created by the antiporter, and a steady state is reached within one minute (Fig. 5b). In the presence of a counter ion (valinomycin in the presence of K^+) the rate increases by 4–5 times. A167P under similar conditions hardly reacts to the change in $\Delta\Psi$.

3.1.4. Structure-based deletion of the NhaA β-sheet

The availability of the crystal structure has facilitated the rational design of site-directed deletions, although these are risky because of possible structural damage.

Many transporters and channels exist in the native membrane as oligomers [91]. In most cases, the functional/structural role of the oligomeric state is still unknown. Several experimental approaches have strongly suggested that NhaA is a dimer in the native membrane; these experimental approaches include genetic complementation [24], biochemical pull-down experiments [24], intermolecular cross-linking [24], electron spin resonance (ESR) studies [25,26] and cryo-electron microscopy of 2D crystals [27,28].

The question of whether the dimeric state of NhaA is essential for its structure and/or function in Na^+/H^+ exchange and/or pH regulation was elusive until recently, when we constructed a deletion mutant of NhaA that encodes monomeric NhaA [92]. This mutant enabled a comparison to be made, for the first time, between the functionalities of monomeric and dimeric NhaA [35,92].

The crystal structure of NhaA revealed a β-hairpin located on the periplasmic side of the membrane; this β-hairpin has been proposed to form the dimer interface [21,26,28,93] (Fig. 1a). In line with this prediction, strong intermolecular cross-linking in the native membrane was identified between two Cys replacements, each localized in one β-hairpin [35]. ESR studies also supported these results [26].

On the basis of these observations, we therefore constructed an NhaA mutant, NhaA/Δ(P45-N58), deleted of the β-hairpin. We found that the NhaA/Δ(P45-N58) protein exists exclusively in a monomeric form both in the native-membrane proteoliposomes and in DDM micelles. Most importantly, even under routine stress conditions of growth (0.1 M LiCl or 0.6 M NaCl at pH 7 and 0.6 M NaCl at pH 8.3), the monomeric mutant conferred growth resistance and exhibited pH-regulated

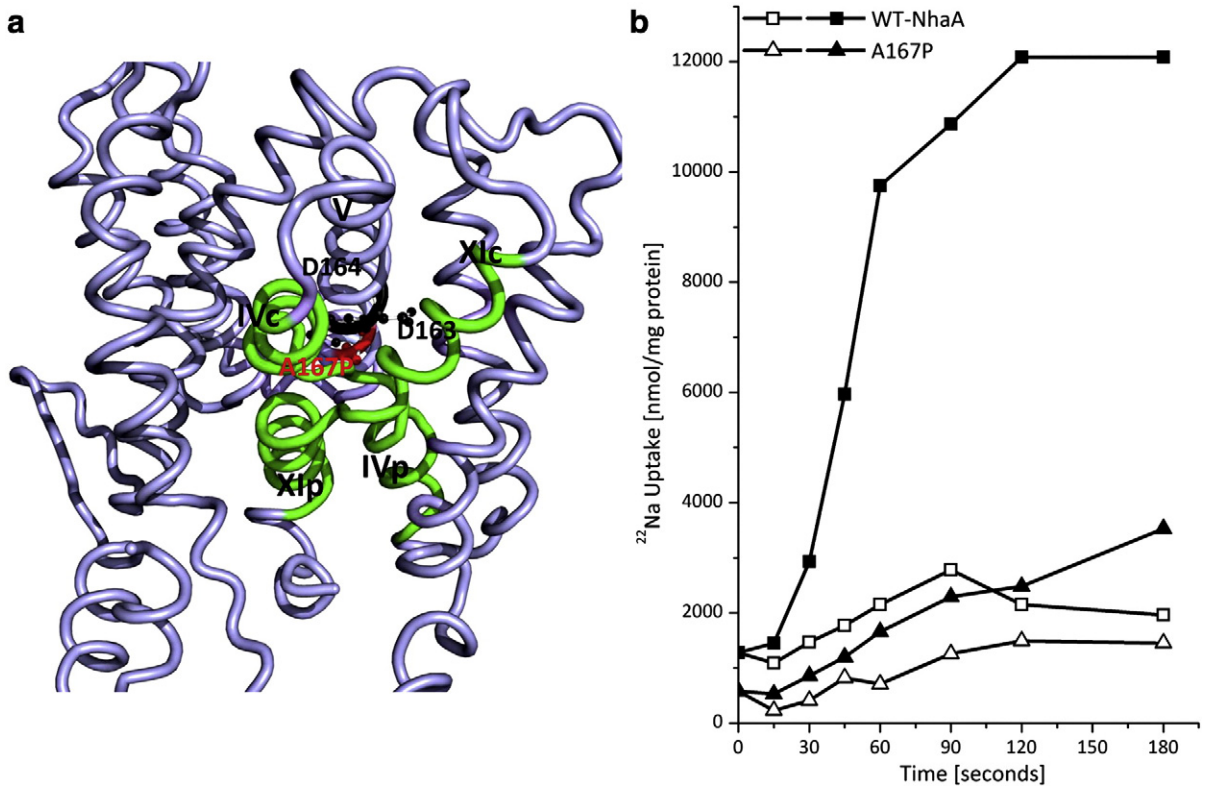

Fig. 5. NhaA mutant – A167P – is indifferent to membrane potential. (a) The mutant A167P (TM V) is shown on the structure (cartoon representation). D163 and D164 are shown in black, at the putative active site. (b) A comparison of ΔpH-driven ^{22}Na uptake of wild-type NhaA and variant A167P, purified proteins reconstituted in proteoliposomes. In the presence of a co-ion (valinomycin in the presence of K^+; full symbol) the uptake rate of wild-type NhaA dramatically increases, as expected for an electrogenic antiporter, whereas the uptake of the mutant hardly changes [94].

Na^+/H^+ antiport activity very similar to that of the wild-type dimeric NhaA [92,94]. Strikingly, under more extreme stress conditions (pH 8.5 in the presence of 0.7 M NaCl or 0.1 M LiCl), monomeric NhaA/(Δ(P45-N58) is much less efficient than wild-type dimeric NhaA in conferring growth resistance. Hence, the dimerization of NhaA is important for the stability of the antiporter.

Aside from the β-sheet interaction at the periplasmic face of the membrane, structural studies have shown several additional interactions at the cytoplasmic face between helix VII (Arg204, Ley210) of one monomer and helix IX (Trp258) of the other [93,28]. The fact that deletion of the β-sheet was enough to produce monomers suggests that these contacts are less crucial for the dimer [92].

4. The dynamic segments of NhaA protein that change conformation in response to pH and/or ligands

As described above (Section 3), NhaA is a "nano-machine" that changes conformations during activity to exchange $2H^+$ for $1Na^+$ across the membrane, and its activity is tightly regulated by pH. As yet, only one conformation of NhaA has been structurally determined: down-regulated NhaA in acidic pH [21] and (PDB IDs: 4AU5, 4ATV; preliminary results of Cameron, A., and Drew, D. and Fig. 1a).

To understand the mechanism of activity and its pH regulation, it is crucial to identify all active conformations of NhaA. Below we review a number of approaches that have been used to obtain information on these conformations.

4.1. Crystallography

4.1.1. X-ray crystallography

Notwithstanding remarkable recent advances in cryo-electron microscopy and nuclear magnetic resonance (NMR) approaches, as yet, the most successful way to determine the atomic structure of a membrane protein is X-ray crystallography. To determine the structure of NhaA in its active conformations, it is necessary to obtain crystals that diffract X-rays at alkaline pH, because NhaA is active and binds its ligands only at pH levels between 7 and 8.5 [3,17,33]. Our group has already obtained 3D crystals at pH 7.5 that diffract X-rays at 5.1 Å resolution (in collaboration with Tsuyoshi Nonaka and Hartmut Michel, Max Planck Institute of Biophysics, Frankfurt, Germany, unpublished results). The structure revealed the backbone of the NhaA dimer, which is in line with a projection map previously obtained by cryo-electron microscopy of 2D crystals [27,95]. The monomeric helix packing of the dimer crystal structure is very similar to that observed in the crystal structure at pH 4 [93]. Importantly, the results show that NhaA crystallizes at alkaline pH, although, as yet, at low resolution.

On the basis of our numerous prior attempts to crystallize NhaA at alkaline pH, it has become apparent that the acidic pH locked conformation of NhaA is energetically preferable for crystallization. Indeed, the most recent crystal structure of NhaA was determined at pH 3.5 (see Section 2.1). Similar difficulties have been encountered with LacY [96] and other transporters. There are two main approaches to overcoming this problem. One is to use fluorescence-based methods to screen homologues in the evolutionary clade for their suitability for structural studies [97–99]. Indeed, Drew and colleagues recently determined the structure of NapA [29], a remote homologue of NhaA (less than 15% identity, see Sections 2.2.1 and 5.2.1). The other approach is trapping and/or stabilizing an active conformation of the transporter as described below.

4.1.1.1. Bicelles and lipidic-cubic-phase-(LPC) based crystallization. These methods maintain the lipid environment of the membrane protein and therefore may stabilize the transporter [100–103] Most

importantly, LPC has recently been successful with secondary transporters [48,49,104].

4.1.1.2. Fixing an active conformation. It is possible to fix a conformation by cross-linking. This has been done, for example, with a bacterial homologue of the eukaryotic glutamate transporters from *Pyrococcus horikoshii*, Glt_{Ph} [45]. Another approach utilizes inhibitors [105,106].

Co-crystallization of membrane proteins with monoclonal antibody (mAb) fragments increases the area for crystal contacts and stabilizes a single conformation, both necessary for obtaining well-diffracting crystals [107]. A number of mAbs specific to native conformations of NhaA are already available [108]. One of them fixes only an active conformation of NhaA [109].

4.1.1.3. Rational design of stable mutants for crystallization in new conformations and/or improving diffraction resolution

4.1.1.3.1. NhaA mutants with increased stability. The SERp server (http://nihserver.mbi.ucla.edu/SER/) can be used to predict how mutagenesis reduces surface entropy in the structure of a membrane protein. Lowering the entropy is supposed to improve crystallization. Following SERp's computations, and guided by the NhaA crystal structure at pH 4, we have identified several charged residues that can potentially be mutated to decrease the entropy of NhaA and produce crystal contacts with greater stability.

4.1.1.3.2. NhaA mutants stable at higher temperatures. Better-diffracting crystals are obtained from mutants of membrane proteins that are stable at higher temperatures [110]. High-temperature-stable NhaA mutants can be detected using the micro-scale fluorescent thermal stability assay [111]. This method is based on thiol-specific fluorochromes such as CPM (N-[4(7-diethylamino-4-methyl-3-coumarinyl)phenyl]maleimide), which fluoresce only upon binding to SH. This method was easily applied to determine the melting point of NhaA (61 °C), because the native three NhaA Cys residues were shown to be accessible to SH reagents only after denaturation [77]. Another effective approach is to look for homologues in thermophilic bacteria [29,112].

4.1.1.3.3. Using molecular genetics to trim tails and loops that appear unstructured in the NhaA crystal structure. The N- and C-termini of NhaA were not resolved in the crystal structure [21], suggesting instability of these segments. Previous studies have shown that trimming such parts can be very helpful towards crystallization [112].

4.1.2. Cryo-electron microscopy of 2D crystals

Cryo-electron microscopy of 2D crystals is a very good approach for studying conformational changes of membrane proteins. This is because in 2D crystals, the protein is embedded in lipids, the native environment. However, as yet, this technique has yielded very few high-resolution structures. Cryo-electron microscopy of 2D NhaA crystals [27,95] revealed the antiporter's dimeric structure and the number of helices, but only upon determination of the NhaA 3D crystal structure were helix assignment, topology and side-chains revealed [21].

Two sequential conformational changes in NhaA were identified through cryo-electron microscopy of 2D NhaA crystals grown at acidic pH and then incubated at alkaline pH [28]. The first change has been suggested to reflect the pH activation of NhaA. It was induced by a rise in pH from 6 to 7 and involved a local ordering of the N-terminus. The second change has been suggested to reflect cation translocation. It was induced by exposure to the ligands Na^+ and Li^+ at pH above 7 and involved displacement of helix IVp toward helix V. Cryo-electron microscopy of 2D crystals also revealed pH-induced structural changes in the hyperthermophilic archaeon Na^+/H^+ antiporter from *Methanococcus jannaschii*, $NhaP1_{MJ}$ [59].

4.1.3. Peptide amide hydrogen-deuterium exchange mass spectrometry

Chung and colleagues recently introduced an interesting approach for identifying dynamic domains in membrane proteins [113]. The rate of exchange of the amide hydrogens in a protein are a function of the protein's thermodynamic stability, i.e., the stability of the hydrogen bonds that each amide forms in the protein's native structure. Changes in exchange rates reflect bonds' propensity to form or to be disrupted, thereby providing information about protein structural changes.

4.2. In silico predictions of conformational changes

Determination of the crystal structure of NhaA paved the way for structure-based computational modeling of dynamic domains. It is crucial to validate experimentally that the computational predictions are realized in situ in the membrane. This has been achieved with all computations applied to NhaA [13,114].

4.2.1. MCCE analysis and MD simulation

Multiconformation continuum electrostatics analysis (MCCE) enables multiple positions of side-chain rotamers, hydroxyl protons and water protons to be incorporated into the calculation of the pH dependence of the ionization equilibria of titratable groups, providing the pK_a values of the ionizable residues. Results of an MCCE study with NhaA revealed clusters of electrostatically tightly interacting residues in transmembrane arrangement [115]. Many residues in the "pH sensor" (see Section 3.1.1) domain have extreme pK_a values, suggesting that no change occurs in the protonation state of these residues within the physiological pH range, unless the NhaA structure is altered. Glu78 in the pH sensor, with pK_a near the physiological range, is suggested to trigger such pH-dependent structural change. Furthermore, the two essential aspartates in the active site (Asp163 and Asp164) remain protonated until pH activates NhaA. The importance of the electrostatic network in pH activation of NhaA has been validated experimentally [114].

Molecular dynamics (MD) simulations are a powerful tool in computational investigations of protein dynamics. MD simulations were used to study the dynamic behavior of the hydrogen-bonded network in NhaA under a shift in pH from 4 to 8 [116]. The helical regions preserved the general architecture of NhaA throughout the pH change, a prediction that has been experimentally validated [80]. In the loop regions, in contrast, large conformational drifts were predicted to occur upon alkaline shift to pH 8, as has been observed biochemically [109,117] and biophysically [80,81]. Increased flexibility of TM IV was also predicted [116] and verified by cryo-electron microscopy of 2D crystals [28] and biochemically [47]. The barrier observed between the funnels at acidic pH was penetrated by water and a remarkable conformational reorganization was identified in TM X [114,116]. Accordingly, a pH-dependent movement of Lys300 was verified by cross-linking [23]. MD simulations have also contributed towards the development of a model for the dynamics of NhaA during pH regulation and exchange activity [34].

4.2.2. Computation based on pseudo-symmetry of the protein structure and elastic network analysis predicts a pH-induced conformational change in NhaA

Using two computational approaches—pseudo-symmetry analysis and elastic network analysis—we have explored the conformational change that NhaA undergoes following pH elevation to alkaline ranges. First, on the basis of pseudo-symmetric features of the NhaA crystal structure [118,13], our proposed model for NhaA at alkaline pH includes a closed cytoplasmic funnel, and a periplasmic funnel of extended volume, in contrast to the cytoplasmic-open conformation revealed by the crystal structure [21]. To examine the transporter's functional direction of motion, we conducted elastic network analysis of the crystal structure and detected two main normal modes of motion. Notably, the results of the pseudo-symmetry analysis and the elastic network analysis predicted similar trends of conformational changes, consisting of an overall rotational, twisting motion of the two domains around a putative symmetry axis passing approximately through the funnel

centers, perpendicular to the membrane plane. This motion, along with conformational changes within specific helices, results in closure at the cytoplasmic end and opening in the periplasmic end. These predictions, validated by cross-linking experiments, suggest that the model structure and motion depict alkaline pH-induced conformational changes, mediated by a cluster of evolutionarily conserved, titratable residues, at the cytoplasmic ends of TMs II, V and IX.

4.3. Identifying conformational changes in situ in the membrane

4.3.1. Test of accessibility of a membrane protein to various probes as a function of changes of a specific experimental condition

Accessibility to trypsin, or to other proteases, is monitored by digestion of the protein. When the digestion pattern changes as a function of a specific change in a particular experimental condition, the specific change, most likely, induces a conformational change in the protein. For example [117,119], NhaA has many putative trypsin recognition sites according to the primary structure, but only one of them at Lys249 in TM IX is cleaved by trypsin and only at alkaline pH. Importantly, the pH profile of the digestion reflects the pH dependence of the NhaA antiport activity [117,119]. Hence, digestion of NhaA by trypsin revealed a pH-induced conformational change in NhaA at TM IX.

Accessibility to mAbs directed against the target protein is monitored by assaying binding of the mAbs to the protein. Several mAbs specific to NhaA have been isolated [108], and their epitopes have been mapped [120]. The binding of mAb 1F6 to NhaA revealed a pH-induced conformational change of NhaA at the N-terminus [109]. This finding has recently been verified by cryo-electron microscopy of 2D crystals [28].

4.3.2. Test of accessibility of site-directed Cys replacements to various probes as a function of changes in a specific experimental condition

Many biophysical and biochemical approaches in the study of structure–function relationship in membrane proteins *in situ* are based on replacement of an amino acid with Cys in a target protein that has been engineered as Cys-less (CL). NhaA cysteines, like those of many other membrane transport proteins [74], can be replaced with other amino acids, with minor effect on activity [77]. Cys replacements are inserted site-specifically in CL-NhaA, and the effect of the replacement on the functionality of the protein and its pH dependence is subsequently studied (Cys-scanning, see Section 3.1.1). Furthermore, the Cys replacement in CL-NhaA allows various SH reagents to be used to probe the protein site-specifically for different properties, without background interference from native cysteines. Tests of accessibility of Cys replacements to various membrane permeant probes are often carried out using NEM (N-ethylmaleimide). NEM ethylates Cys in the presence of water; therefore, the NEM-accessibility assay traces water-filled cavities in the protein. Charged and membrane-impermeant probes such as $MTSES^-$ (2-sulfonatoethyl methanethiosulfonate) and $MTSET^+$ ((2-(trimethylammonium)-ethyl)methanethiosulfonate) are used to identify residues that are exposed on the protein surface or connected via water-filled funnels to the environment water space [74].

Cys-replacement-based assays using various probes have identified locations on NhaA that change conformation with pH. A test of the accessibility of Cys-replacement E252C on TM IX to the membrane permeant fluorescent probe MIANS (2-(4′-maleimide-anilino)-naphthalnene-6-sulfonic acid) showed that E252C changes conformation with pH [81] in a pattern very similar to the pH profile of NhaA activity. Exposure to ligands (Na^+ and Li^+) also induced conformational change in E252C. Tests of the accessibility of Cys replacements on TM IX and II to various probes revealed that the cytoplasmic funnel deepens at alkaline pH as compared to acidic pH [80] and that E65C on TM II changes conformation with pH [78]. Remarkably, similar pH profiles were obtained for pH-induced conformational changes and for NhaA activity observed *in situ*.

Finally, most recently [47], the use of Cys replacements has revealed that the extended chain of TM IV changes conformation with pH (Fig. 6). In particular, Cys replacements were inserted into TM IV of NhaA (the extended chain connecting the small helices IVp and IVc), and the accessibility of these Cys replacements to the positively charged SH reagent [2-(trimethyammonium)ethyl] methanethiosulfonate bromide (MTSET)s was evaluated in intact cells at pH 8.5 and at pH 6.5. These tests revealed the following: (a) Cys replacement of the most conserved residues of TM IV strongly increases the apparent K_m of NhaA to both Na^+ and Li^+; (b) the cationic passage of NhaA at physiological pH is lined by the most conserved and functionally important residues of TM IV; (c) a pH shift from 6.5 to 8.5 induces conformational changes in helix IVp and in the extended chain at physiological pH.

4.3.3. Estimation of intra-molecular distances between pairs of Cys replacements, as a function of changes in a specific experimental condition

The distance between two Cys replacements can be estimated using bifunctional cross-linking reagents of fluorescent (FRET, Fluorescence Energy Transfer) or EPR (Electron Paramagnetic Resonance) probes of known length. If a change in a particular experimental condition influences the distance between two Cys replacements, then it is possible to conclude that the change induces a conformational change in the protein. We carried out such an experiment to identify pH-induced conformational changes in NhaA. The study revealed that at alkaline pH the distance between the conserved center of helix X and E78 of TM II is drastically lower compared with that in the crystal structure at pH 4 [23], implying that a pH-induced conformational change takes place in one or both helices. In a study based on EPR techniques, singly spin-labeled mutants of NhaA were used to determine distances between NhaA monomers as a function of pH. These experiments showed that the structure at the monomer-monomer interaction changes only moderately with pH [25].

5. Functional dynamics; the kinetics of the conformational changes

5.1. Paving the way to functional dynamics of NhaA with site-directed Trp fluorescence

An understanding of the kinetics of the conformational changes of NhaA is crucial in order to decipher the antiporter's turnover cycle and its pH regulation. For this purpose we constructed functional Trp-less NhaA with Phe residues replacing the eight Trps of the native antiporter [121] (Fig. 7). We used the Trp-less NhaA, showing no Trp fluorescence, to site-specifically insert a single Trp (F136W on TM IVc) in order to monitor conformational changes of TM IVc and F399W at the active site (TM XI) (Fig. 7).

With single Trp/F136W (Fig. 7d) a change from pH 6.0 to 8.5 induces a red shift and dramatically increases fluorescence in a reversible fashion, and no effect is observed when either Na^+ or Li^+ is added. In marked contrast, with single Trp/F339W (Fig. 7c) changes in pH do not alter fluorescence, but the addition of either Na^+ or Li^+ drastically quenches fluorescence at alkaline pH. Therefore, the Trp at position 136 specifically monitors a pH-induced conformational change that activates NhaA, while the Trp at position 339 senses a ligand-induced conformational change that does not occur until NhaA is activated at alkaline pH. Because of the rapid kinetics of NhaA we now use stopped-flow spectrofluorimetry to determine the kinetics of the pH-induced and ligand-induced conformational changes.

5.2. Dynamic model of NhaA Na^+/H^+ antiporter activity

A common property of standard biochemical transport assays is a long measurement time, ranging from seconds to minutes. This property applies to crystallography, which provides invaluable snapshots of structures of different conformations but with little or no information regarding the time scale of the transitions. The following approaches

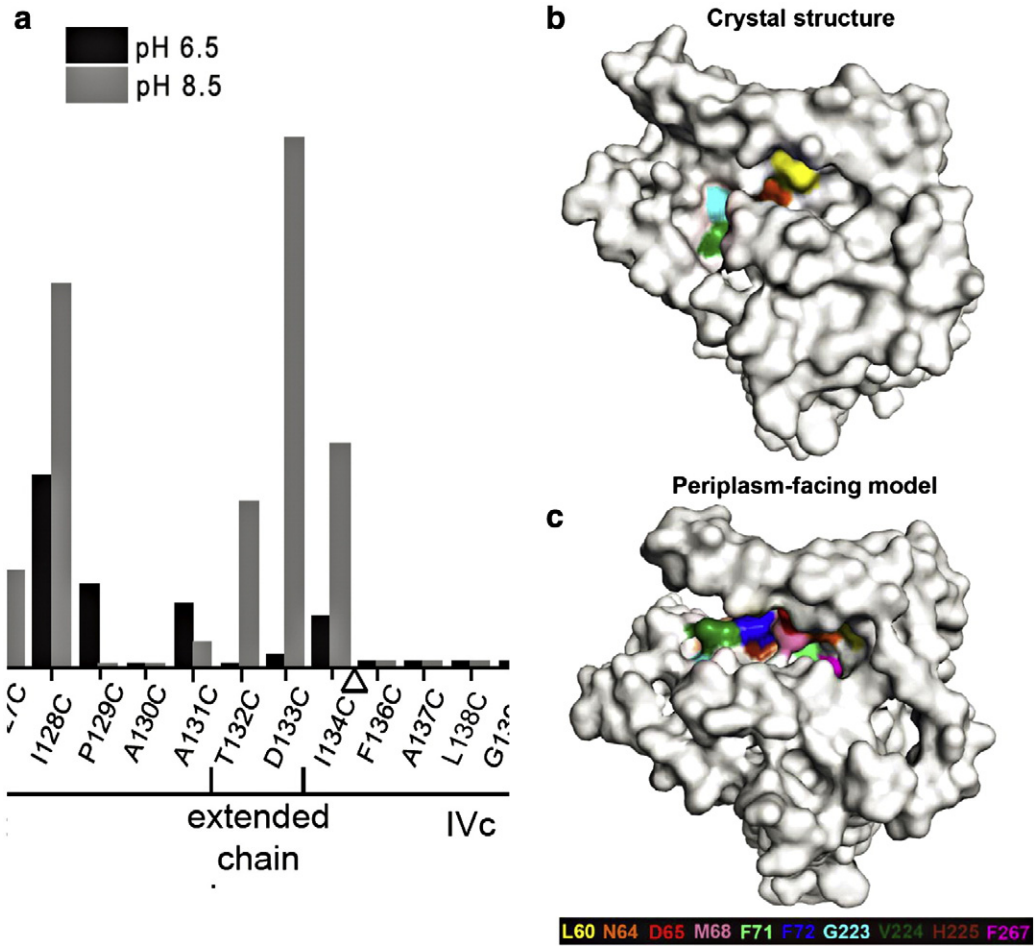

Fig. 6. pH-induced conformational change of the extended chain in NhaA TM IV. (a) Intact cells expressing the Cys-replacement mutants in TM IV of Cys-less NhaA were incubated with MTSET at pH 6.5 and pH 8.5. Proteins were purified by Ni^{+2}–NTA affinity chromatography and labeled on the beads with fluorescein-maleimide to estimate the percentage of free Cys remaining after modification with MTSET (for further details see Section 4.3.2 and [47]). (b) Accessibility measurements of Cys mutants mapped on the crystal structure and the periplasmic-facing model (c) shown in surface representation. The exposure of the extended chain of TM IV is shown in dark red. The data were obtained from [47,78–80], (Section 4.3.2).

have been used to overcome this limitation and to derive insights regarding the dynamics of NhaA antiport activity.

5.2.1. Dynamic model of NhaA antiport activity based on the structures

The down-regulated inward-open conformation of NhaA, crystallized at pH 4 ([21] and 2.1.1.) and the outward-open active conformation of NapA, crystallized at pH 7.8 ([29] and Section 2.2.1), and the major structural differences between them, served as the basis for a model of the mechanism of NhaA-mediated antiport. In the dimerization interface, which seems likely to remain stable during transport across the membrane [25,28,92], the core domain in the NhaA crystal structure is rotated by 21° relative to the core of the NapA structure. Such a large rotation of the core domain is proposed to close the cavity seen on the outside of NapA and to open the cytoplasmic funnel on the inside, as observed in NhaA. During this time the two cation binding aspartates (Asp156 and Asp157 in NapA; Asp163 and Asp164 in NhaA) are shifted 10 Å towards the cytoplasmic surface of the transporter. This elevator movement of a substrate-binding domain carries the ions from one side of the membrane to the other in exchange for protons. Hence, the alternating-access mechanism of NhaA requires a surprisingly large rotation and movement of the core domain against the dimerization domain despite the very fast transport rate measured biochemically for NhaA [17].

The suggested model resembles that of the transport mechanism of Glt_{ph} [45], which is a version of the two-domain rocking bundle model [122]. The latter model was also proposed for the bile acid Na^+ symporter $ASBT_{NM}$, a structural homologue of NhaA and of NapA ([30] and (Section 2.2). A two-domain transport mechanism was also recently predicted for the pH-induced conformational change of NhaA, on the basis of the two inverted repeats, as well as data from elastic network modeling and biochemical cross-linking experiments ([123] and Section 4.2.2). Importantly, this model does not predict the movement of the ligand-binding domain but rather the pH-induced movement. Hence, it does not support the mechanistic elevator model.

It is clear that capturing multiple distinct conformations of a given transporter is an essential step in elucidating the transport mechanism. Unfortunately, as yet, such a task has proven challenging to accomplish for many transporters (see above, Section 4.1) and instead, comparative analysis has been used to obtain such information, for the NhaA transporters as for other many transporters [37]. Additional structures and rapid assays of transport kinetics are needed to clarify how ion binding and release is coupled to the structural changes.

5.2.2. A kinetic model of NhaA activity based on electrophysiology

To obtain rapid-kinetics information on NhaA's transport activity, we undertook an electrophysiological approach, SSM-based electrophysiology (SSM = solid supported membrane). This approach allowed us to measure the NhaA activity at a resolution of milliseconds, under well-defined conditions on both sides of the membrane. Using Na^+ or H^+ gradients as the driving source [68,69,124], translocation of charge by NhaA was measured directly by tracing transient currents generated in NhaA proteoliposomes, absorbed onto the SSM [68,69,124] (Fig. 8). Forward (Na^+ excreted from the cytoplasm) and reverse (Na^+ taken up to the cytoplasm) transport directions were investigated using

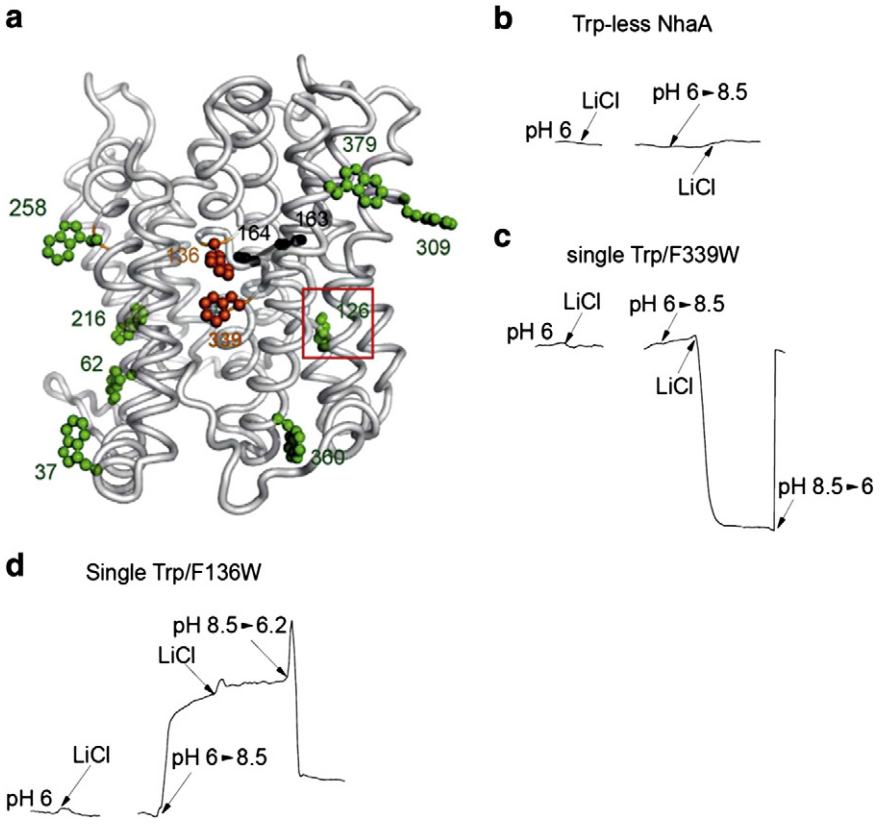

Fig. 7. Site-directed Trp fluorescence reveals two different conformational changes in TM IV. (a) The native eight Trps of NhaA are shown in green (ball and stick) on the structure (tube representation) with the Trp replacements F136W and F339W (red). (b–d) The indicated proteins were affinity-purified and resuspended (0.45–0.50 μM) in reaction mixture containing 5 mM $MgCl_2$, 20–50 mM BTP, 150 mM choline chloride, 10% sucrose and 0.015% dodecyl maltoside. The Trp fluorescence emission was measured with the time-dependent mode of the spectrofluorimeter (PerkinElmer). For each variant two experiments were conducted in parallel: Left, after steady state was reached at pH 6, LiCl (10 mM) was added. Right, after steady state was reached at pH 6, the pH was changed from pH 6 to 8.5 and incubation continued to reach a new steady state. Then, LiCl (10 mM) was added and incubation continued followed by changing the pH back to 6. The wavelengths were 295 nm excitation and the emission was at the peak of each variant; 344, 345, and 338 nm for Trp-less NhaA, single Trp/F136W and single Trp/F339W, respectively [121] and (Section 5.1).

preparations of transporters with inside-out orientations (membrane vesicles) and with right-side-out orientations (NhaA proteoliposomes), respectively [68,69] (Fig. 8a).

Our experiments showed that NhaA is a symmetric transporter and contributed towards the development of a kinetic model of the NhaA translocation cycle. This model supports the alternate accessibility mechanism of secondary transporters [60], wherein a single binding site alternates across the membrane. The translocation process includes an electrogenic-rate-limiting step in which Na^+ is transferred across the membrane while bound to the aspartates of the binding site (Asp163, Asp164), and an electroneutral step transporting H^+ across the membrane while bound to the aspartates (Fig. 8b). H^+ and Na^+ compete for the single binding site, and the competition explains many phenomena of NhaA pH regulation.

Two mechanisms for pH regulation of NhaA have been proposed. The first is an allosteric mechanism [14] where a "pH sensor" located far from the active site accepts the pH signal and transduces it to activate a conformational change in NhaA. A similar mechanism has also been proposed for the eukaryotic Na^+/H^+ antiporters (reviewed in [6,9,19,20]). We have identified clusters of amino acids remote from the active site that, when mutagenized, abrogate or change the pH profiles of NhaA; these clusters, in addition to the identification of two conformational changes, one pH-induced and the other ligand-induced [121], strongly support the proposed mechanism.

The second proposed mechanism of NhaA pH regulation is a direct competition of Na^+ and H^+ for the active site. Results of electrophysiological experiments lend strong support to this proposition. These experiments indicate that the decrease in transport activity at acidic pH values is due to an increase in K_m^{Na} and not due to a decrease in v_{max} [69]. Furthermore, lowering the pH to pH 5 at the sodium release side does not inactivate NhaA either in the forward mode or in the reverse mode, showing that even at pH 5 NhaA does not adopt an inactive conformation at either the cytoplasmic or periplasmic side.

In an attempt to reconcile the two proposed mechanisms, we analyzed a number of different NhaA variants, modulating the pH profile of the transporter using SSM-based electrophysiology [94]. We found that the kinetic properties of monomeric and dimeric NhaA are identical, and that the site-specific mutations affected NhaA activity in substantially different ways by changing (i) the properties of the binding site or (ii) the dynamics of the transporter. In the first case pK and/or K_D^{Na} were altered; in the second case the rate constants of the conformation transition between the inside- and the outside-open conformations were modified. We found that residues as far apart as 15–20 Å from the binding site can have a significant impact on the dynamics of the conformational transitions or on the binding properties of NhaA. Finally, we functionally characterized the mutant A167P. This mutation is located in TM V in close proximity to the cation binding site (Fig. 5a). Surprisingly, this novel mutant did not show the characteristic property expected for an electrogenic transporter; whereas wild-type NhaA with a stoichiometry of $2H^+/1Na^+$ is extremely sensitive to change in the membrane potential, A167P is hardly affected (Fig. 5b). These results suggest that the mutation either affects the Na^+/H^+ stoichiometry of the mutant or changes the rate-limiting step of the antiport cycle from an electrogenic to an electroneutral step [94].

Importantly, as summarized in Table 1, there are differences between the results obtained by electrophysiology and those obtained by classical transport assays (ΔpH-driven $^{22}Na^+$ uptake in proteoliposomes; respiration-driven Na^+ uptake in everted membrane vesicles

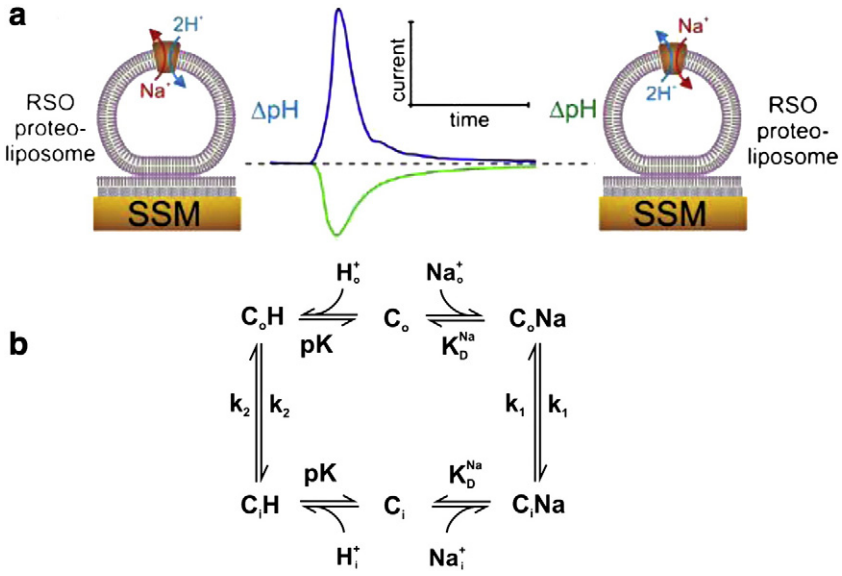

Fig. 8. Electrophysiology of NhaA. (a) The forward transport mode of NhaA corresponding to its physiological transport direction is shown on the left, and the reversed transport mode is shown on the right. In the middle, the transient currents driven by Na gradient (ΔNa^+) or ΔpH, as observed in the SSM, are schematically depicted. (b) A minimal kinetic model used for the analysis of the transport properties of NhaA as revealed by the SSM (details in [69] and Section 5.2.2). The outward-facing transporter C_O binds substrates either H_O or Na_O from the periplasm. The inward-facing carrier, C_i binds the ligands from the cytoplasm. The conformational transitions CoH ↔ CiH and CoNa ↔ CiNa are associated with a displacement of the two negatively-charged aspartate residues and one Na^+ or two H^+, respectively. In the case of Na^+ translocation this leads to a net charge displacement and is suggested to be the rate-limiting step.

using acridine orange or similar fluorescent probes of ΔpH). The two proposed mechanisms of pH regulation described above (Section 5.2.2) obviously represent different mechanistic concepts, although they are not mutually exclusive, and the conformational transitions they rely on are not necessarily different. We believe that the differences in time resolution of the assays (electrophysiology, milliseconds; biochemistry, seconds) and driving forces (electrophysiology, chemical gradient; biochemistry, PMF) of the transport assays are the main factors driving the differences observed (Table 1). Indeed, recently, a partial reaction was identified in NhaA by the SSM method ([69] and Fendler, K. and Padan, E., unpublished results).

In sum, as yet there is no answer as to how NhaA is pH-regulated at the molecular level. It is important to note that given the ligand exchange mechanism, competition between the ligands, Na^+ and H^+, is expected to take place. The question remaining is whether in addition to the competition there is a pH-induced activation step. To resolve this issue, further studies are required, e.g., studies using stop flow devices to measure transport activity, as was done for LacY [125,126]. Such studies can overcome the time-gap between biochemistry and electrophysiology.

Notably, an elegant and integrated approach has recently been developed to investigate the dynamics of the conformational changes that are associated with substrate binding and transport of LeuT, a neurotransmitter transporter homologue [127]. Single-molecule fluorescence resonance energy transfer (smFRET) was used to quantify time-dependent changes in the LeuT structure, which might otherwise have been masked by ensemble-averaging in bulk measurements or suppressed through crystallographic conditions. Computational methods were applied in parallel to assess the mechanistic context of the observed conformational changes [128].

6. Conclusions

The crystal structure of down-regulated NhaA crystallized at acidic pH 4 [21] has provided the first structural insights into the antiport mechanism and pH regulation of an Na^+/H^+ antiporter [22]. On the basis of the NhaA crystal structure [21] and experimental data (reviewed in [2,22,38]), we have suggested that NhaA is organized into two functional regions: (i) a cluster of amino acids responsible for pH regulation, and (ii) a catalytic region at the middle of the TM IV/XI assembly, containing unique antiparallel unfolded regions that cross each other, forming a delicate electrostatic balance in the middle of the membrane. This unique structure contributes to the cation binding site and facilitates the rapid conformational changes expected for NhaA. Although extended chains interrupting helices have since emerged as a common feature for ion binding in transporters, the NhaA fold, shared by $ASBT_{NM}$ [30] and NapA [29], is unique among these structures. Computational [13,34], biochemistry [33,38,47] and electrophysiological methods [69] have been used to develop intriguing models for the mechanism of NhaA. However, the conformational changes and the residues involved have not yet been fully identified. Another issue that remains an enigma is how energy is transduced in

Table 1
Differences in results obtained by electrophysiology and standard biochemical assays of NhaA activity.

	Biochemistry	Electrophysiology
Time scale of assay	Seconds–minutes[1]	Miliseconds[2,3]
Driving force	Electrochemical Na^+ or H^+ gradients[4] ($\Delta\mu_{Na+}$, $\Delta\mu_{H+}$)	Chemical[3] Na^+ gradient or H^+ gradient
Apparent K_m for Na^+	0.2–0.5 mM[4]	10–100 mM[3]
Increase in V_{max} with pH	1000 fold[1]	1.5 fold[3]
The lowest pH of Na^+ transport	pH 6[5,6]	pH 5[3]
Rate-limiting step	The proton loaded carrier[7]	The Na^+ loaded carrier[3]
Conformational changes	A pH induced is separated from a ligand induced[8]	
The effect of a change in $\Delta\Psi$ on transport rate	Very strong[4,9]	Cannot be measured

Legend: The prefix numbers refer to the references from which the information was taken: 1) [17]; 2) [68]; 3) [69]; 4) [18]; 5) [17]; 6) [14]; 7) [129]; 8) [121]; 9) [69].

this "nano-machine". We expect that an integrative approach will reveal the residues that are crucial for NhaA activity and regulation, as well as elucidate the pH- and ligand-induced conformational changes and their dynamics. Ultimately, integrative results will shed light on the mechanism of activity and pH regulation of NhaA, a prototype of the CPA2 family of transporters.

Acknowledgement

EP thanks the Israel Science Foundation (grant No. 284/12).

References

[1] E. Padan, T.A. Krulwich, Sodium stress, in: G. Storz, R. Hengge-Aronis (Eds.), Bacterial Stress Response, ASM Press, Washington, D. C., 2000
[2] T.A. Krulwich, G. Sachs, E. Padan, Molecular aspects of bacterial pH sensing and homeostasis, Nature reviews, Microbiology 9 (2011) 330–343.
[3] E. Padan, L. Kozachkov, Conformational changes in NhaA Na^+/H^+ antiporter, Mol. Membr. Biol. 30 (2012) 90–100.
[4] I.C. West, P. Mitchell, Proton/sodium ion antiport in Escherichia coli, Biochem. J. 144 (1974) 87–90.
[5] E. Padan, T. Tzubery, K. Herz, L. Kozachkov, A. Rimon, L. Galili, NhaA of *Escherichia coli*, as a model of a pH-regulated Na^+/H^+antiporter, Biochim. Biophys. Acta 1658 (2004) 2–13.
[6] J. Orlowski, S. Grinstein, Emerging roles of alkali cation/proton exchangers in organellar homeostasis, Curr. Opin. Cell Biol. 19 (2007) 483–492.
[7] G. Speelmans, B. Poolman, T. Abee, W.N. Konings, Energy transduction in the thermophilic anaerobic bacterium Clostridium fervidus is exclusively coupled to sodium ions, Proc. Natl. Acad. Sci. U. S. A. 90 (1993) 7975–7979.
[8] L. Fliegel, Molecular biology of the myocardial Na+/H+ exchanger, J. Mol. Cell. Cardiol. 44 (2008) 228–237.
[9] J. Orlowski, S. Grinstein, Diversity of the mammalian sodium/proton exchanger SLC9 gene family, Pflugers Arch. 447 (2004) 549–565.
[10] C.L. Brett, M. Donowitz, R. Rao, Evolutionary origins of eukaryotic sodium/proton exchangers, Am. J. Physiol. Cell Physiol. 288 (2005) C223–C239.
[11] M. Landau, K. Herz, E. Padan, N. Ben-Tal, Model structure of the Na+/H+ exchanger 1 (NHE1): functional and clinical implications, J. Biol. Chem. 282 (2007) 37854–37863.
[12] E.R. Slepkov, J.K. Rainey, B.D. Sykes, L. Fliegel, Structural and functional analysis of the Na+/H+ exchanger, Biochem. J. 401 (2007) 623–633.
[13] M. Schushan, A. Rimon, T. Haliloglu, L.R. Forrest, E. Padan, N. Ben-Tal, A model-structure of a periplasm-facing state of the NhaA antiporter suggests the molecular underpinnings of pH-induced conformational changes, J. Biol. Chem. 287 (2012) 18249–18261.
[14] E. Padan, E. Bibi, I. Masahiro, T.A. Krulwich, Alkaline pH homeostasis in bacteria: new insights, Biochim. Biophys. Acta 1717 (2005) 67–88.
[15] E. Padan, M. Venturi, Y. Gerchman, N. Dover, Na^+/H^+ antiporters, Biochim. Biophys. Acta 1505 (2001) 144–157.
[16] Y. Minato, A. Ghosh, W.J. Faulkner, E.J. Lind, S. Schesser Bartra, G.V. Plano, C.O. Jarrett, B.J. Hinnebusch, J. Winogrodzki, P. Dibrov, C.C. Hase, Na+/H+ antiport is essential for Yersinia pestis virulence, Infect. Immun. 81 (2013) 3163–3172.
[17] D. Taglicht, E. Padan, S. Schuldiner, Overproduction and purification of a functional Na^+/H^+ antiporter coded by *nhaA* (*ant*) from *Escherichia coli*, J. Biol. Chem. 266 (1991) 11289–11294.
[18] D. Taglicht, E. Padan, S. Schuldiner, Proton-sodium stoichiometry of NhaA, an electrogenic antiporter from *Escherichia coli*, J. Biol. Chem. 268 (1993) 5382–5387.
[19] L.K. Putney, S.P. Denker, D.L. Barber, The changing face of the Na+/H+ exchanger, NHE1: structure, regulation, and cellular actions, Annu. Rev. Pharmacol. Toxicol. 42 (2002) 527–552.
[20] S. Wakabayashi, T. Hisamitsu, T. Pang, M. Shigekawa, Kinetic dissection of two distinct proton binding sites in Na^+/H^+ exchangers by measurement of reverse mode reaction, J. Biol. Chem. 278 (2003) 43580–43585.
[21] C. Hunte, M. Screpanti, M. Venturi, A. Rimon, E. Padan, H. Michel, Structure of a Na^+/H^+ antiporter and insights into mechanism of action and regulation by pH, Nature 534 (2005) 1197–1202.
[22] E. Padan, The enlightening encounter between structure and function in the NhaA Na(+)– H(+) antiporter, Trends Biochem. Sci. 33 (2008) 435–443.
[23] L. Kozachkov, K. Herz, E. Padan, Functional and structural interactions of the transmembrane domain X of NhaA, Na+/H+ antiporter of Escherichia coli, at physiological pH, Biochemistry 46 (2007) 2419–2430.
[24] Y. Gerchman, A. Rimon, M. Venturi, E. Padan, Oligomerization of NhaA, the Na^+/H^+ antiporter of *Escherichia coli* in the membrane and its functional and structural consequences, Biochemistry 40 (2001) 3403–3412.
[25] D. Hilger, H. Jung, E. Padan, C. Wegener, K.P. Vogel, H.J. Steinhoff, G. Jeschke, Assessing oligomerization of membrane proteins by four-pulse DEER: pH-dependent dimerization of NhaA Na+/H+ antiporter of E. coli, Biophys. J. 89 (2005) 1328–1338.
[26] D. Hilger, Y. Polyhach, E. Padan, H. Jung, G. Jeschke, High-resolution structure of a Na+/H+ antiporter dimer obtained by pulsed EPR distance measurements, Biophys. J. 93 (2007) 3675–3683.
[27] K.A. Williams, U. Geldmacher-Kaufer, E. Padan, S. Schuldiner, W. Kuhlbrandt, Projection structure of NhaA, a secondary transporter from Escherichia coli, at 4.0 A resolution, EMBO J. 18 (1999) 3558–3563.
[28] M. Appel, D. Hizlan, K.R. Vinothkumar, C. Ziegler, W. Kuhlbrandt, Conformations of NhaA, the Na/H exchanger from Escherichia coli, in the pH-activated and ion-translocating states, J. Mol. Biol. 386 (2009) 351–365.
[29] C. Lee, H.J. Kang, C. von-Ballmoos, S. Newstead, P. Uzdavinys, D.L. Dotson, S. Iwata, O. Beckstein, A.D. Cameron, D. Drew, A two-domain elevator mechanism for sodium/proton antiporter, Nature 501 (2013) 573–577.
[30] N.J. Hu, S. Iwata, A.D. Cameron, D. Drew, Crystal structure of a bacterial homologue of the bile acid sodium symporter ASBT, Nature 478 (2011) 408–411.
[31] E.M. Furrer, M.F. Ronchett, F. Verrey, K.M. Pos, Functional characterization of a NapA Na(+)/H(+) antiporter from Thermus thermophilus, FEBS Lett. 581 (2007) 572–578.
[32] N. Kuwabara, H. Inoue, Y. Tsuboi, N. Nakamura, H. Kanazawa, The fourth transmembrane domain of the Helicobacter pylori Na+/H+ antiporter NhaA faces a water-filled channel required for ion transport, J. Biol. Chem. 279 (2004) 40567–40575.
[33] M. Maes, A. Rimon, L. Kozachkov-Magrisso, A. Friedler, E. Padan, Revealing the ligand binding site of NhaA Na+/H+ antiporter and its pH dependence, J. Biol. Chem. 287 (2012) 38150–38157.
[34] I.T. Arkin, H. Xu, M.O. Jensen, E. Arbely, E.R. Bennett, K.J. Bowers, E. Chow, R.O. Dror, M.P. Eastwood, R. Flitman-Tene, B.A. Gregersen, J.L. Klepeis, I. Kolossvary, Y. Shan, D.E. Shaw, Mechanism of Na+/H+ antiporting, Science 317 (2007) 799–803.
[35] K. Herz, A. Rimon, G. Jeschke, E. Padan, Beta-sheet-dependent dimerization is essential for the stability of NhaA Na+/H+ antiporter, J. Biol. Chem. 284 (2009) 6337–6347.
[36] P. Goswami, C. Paulino, D. Hizlan, J. Vonck, O. Yildiz, W. Kuhlbrandt, Structure of the archaeal Na+/H+ antiporter NhaP1 and functional role of transmembrane helix 1, EMBO J. 30 (2011) 439–449.
[37] Y. Shi, Common folds and transport mechanisms of secondary active transporters, Annu. Rev. Biophys. 42 (2013) 51–72.
[38] E. Padan, L. Kozachkov, K. Herz, A. Rimon, NhaA crystal structure: functional–structural insights, J. Exp. Biol. 212 (2009) 1593–1603.
[39] H. Krishnamurthy, C.L. Piscitelli, E. Gouaux, Unlocking the molecular secrets of sodium-coupled transporters, Nature 459 (2009) 347–355.
[40] O. Boudker, G. Verdon, Structural perspectives on secondary active transporters, Trends Pharmacol. Sci. 31 (2010) 418–426.
[41] L.R. Forrest, R. Kramer, C. Ziegler, The structural basis of secondary active transport mechanisms, Biochim. Biophys. Acta 1807 (2011) 167–188.
[42] E. Screpanti, C. Hunte, Discontinuous membrane helices in transport proteins and their correlation with function, J. Struct. Biol. 159 (2007) 261–267.
[43] A. Yamashita, S.K. Singh, T. Kawate, Y. Jin, E. Gouaux, Crystal structure of a bacterial homologue of Na+/Cl−-dependent neurotransmitter transporters, Nature 437 (2005) 215–223.
[44] R. Dutzler, E.B. Campbell, R. MacKinnon, Gating the selectivity filter in ClC chloride channels, Science 300 (2003) 108–112.
[45] N. Reyes, C. Ginter, O. Boudker, Transport mechanism of a bacterial homologue of glutamate transporters, Nature 462 (2009) 880–885.
[46] M. Schushan, M. Xiang, P. Bogomiakov, E. Padan, R. Rao, N. Ben-Tal, Model-guided mutagenesis drives functional studies of human NHA2, implicated in hypertension, J. Mol. Biol. 396 (2010) 1181–1196.
[47] A. Rimon, L. Kozachkov-Magrisso, E. Padan, The unwound portion dividing helix IV of NhaA undergoes a conformational change at physiological pH and lines the cation passage, Biochemistry 51 (2012) 9560–9569.
[48] A.B. Waight, B.P. Pedersen, A. Schlessinger, M. Bonomi, B.H. Chau, Z. Roe-Zurz, A.J. Risenmay, A. Sali, R.M. Stroud, Structural basis for alternating access of a eukaryotic calcium/proton exchanger, Nature 499 (2013) 107–110.
[49] B.P. Pedersen, H. Kumar, A.B. Waight, A.J. Risenmay, Z. Roe-Zurz, B.H. Chau, A. Schlessinger, M. Bonomi, W. Harries, A. Sali, A.K. Johri, R.M. Stroud, Crystal structure of a eukaryotic phosphate transporter, Nature 496 (2013) 533–536.
[50] C. Deisl, A. Simonin, M. Anderegg, G. Albano, G. Kovacs, D. Ackermann, H. Moch, W. Dolci, B. Thorens, A.H. M., D.G. Fuster, Sodium/hydrogen exchanger NHA2 is critical for insulin secretion in beta-cells, Proc. Natl. Acad. Sci. U. S. A. 110 (2013) 10004–10009.
[51] K.C. Kondapalli, L.M. Kallay, M. Muszelik, R. Rao, Unconventional chemiosmotic coupling of NHA2, a mammalian Na+/H+ antiporter, to a plasma membrane H+ gradient, J. Biol. Chem. 287 (2012) 36239–36250.
[52] P. Dibrov, A. Rimon, J. Dzioba, A. Winogrodzki, Y. Shalitin, E. Padan, 2-Aminoperimidine, a specific inhibitor of bacterial NhaA Na(+)/H(+) antiporters, FEBS Lett. 579 (2005) 373–378.
[53] S. Wakabayashi, T. Pang, X. Su, M. Shigekawa, A novel topology model of the human Na(+)/H(+) exchanger isoform 1, J. Biol. Chem. 275 (2000) 7942–7949.
[54] L.D. Shrode, B.S. Gan, S.J. D'Souza, J. Orlowski, S. Grinstein, Topological analysis of NHE1, the ubiquitous Na+/H+ exchanger using chymotryptic cleavage, Am. J. Physiol. 275 (1998) C431–C439.
[55] E.B. Nygaard, J.O. Lagerstedt, G. Bjerre, B. Shi, M. Budamagunta, K.A. Poulsen, S. Meinild, R.R. Rigor, J.C. Voss, P.M. Cala, S.F. Pedersen, Structural modeling and electron paramagnetic resonance spectroscopy of the human Na+/H+ exchanger isoform 1, NHE1, J. Biol. Chem. 286 (2011) 634–648.
[56] M. Schushan, M. Landau, E. Padan, N. Ben-Tal, Two conflicting NHE1 model structures: compatibility with experimental data and implications for the transport mechanism, J. Biol. Chem. 286 (2011) le9(author reply le10.).
[57] B.L. Lee, B.D. Sykes, L. Fliegel, Structural analysis of the Na+/H+ exchanger isoform 1 (NHE1) using the divide and conquer approach, Biochem. Cell Biol. 89 (2011) 189–199.

[58] M. Xiang, M. Feng, S. Muend, R. Rao, A human Na+/H+ antiporter sharing evolutionary origins with bacterial NhaA may be a candidate gene for essential hypertension, Proc. Natl. Acad. Sci. U. S. A. 104 (2007) 18677–18681.
[59] K.R. Vinothkumar, S.H. Smits, W. Kuhlbrandt, pH-induced structural change in a sodium/proton antiporter from Methanococcus jannaschii, EMBO J. 24 (2005) 2720–2729.
[60] O. Jardetzky, Simple allosteric model for membrane pumps, Nature 211 (1966) 969–970.
[61] E.B. Goldberg, T. Arbel, J. Chen, R. Karpel, G.A. Mackie, S. Schuldiner, E. Padan, Characterization of a Na^+/H^+ antiporter gene of *Escherichia coli*, Proc. Natl. Acad. Sci. U. S. A. 84 (1987) 2615–2619.
[62] E. Padan, N. Maisler, D. Taglicht, R. Karpel, S. Schuldiner, Deletion of *ant* in *Escherichia coli* reveals its function in adaptation to high salinity and an alternative Na^+/H^+ antiporter system(s), J. Biol. Chem. 264 (1989) 20297–20302.
[63] E. Pinner, Y. Kotler, E. Padan, S. Schuldiner, Physiological role of *nhaB*, a specific Na^+/H^+ antiporter in *Escherichia coli*, J. Biol. Chem. 268 (1993) 1729–1734.
[64] K. Nozaki, T. Kuroda, T. Mizushima, T. Tsuchiya, A new Na+/H+ antiporter, NhaD, of Vibrio parahaemolyticus, Biochim. Biophys. Acta 1369 (1998) 213–220.
[65] K. Nozaki, K. Inaba, T. Kuroda, M. Tsuda, T. Tsuchiya, Cloning and sequencing of the gene for Na+/H+ antiporter of Vibrio parahaemolyticus, Biochem. Biophys. Res. Commun. 222 (1996) 774–779.
[66] T. Ohyama, K. Igarashi, H. Kobayashi, Physiological role of the chaA gene in sodium and calcium circulations at a high pH in Escherichia coli, J. Bacteriol. 176 (1994) 4311–4315.
[67] E. Padan, S. Schuldiner, Molecular physiology of the Na+/H+ antiporter in Escherichia coli, J. Exp. Biol. 196 (1994) 443–456.
[68] D. Zuber, R. Krause, M. Venturi, E. Padan, E. Bamberg, K. Fendler, Kinetics of charge translocation in the passive downhill uptake mode of the Na+/H+ antiporter NhaA of Escherichia coli, Biochim. Biophys. Acta 1709 (2005) 240–250.
[69] T. Mager, A. Rimon, E. Padan, K. Fendler, Transport mechanism and pH regulation of the Na+/H+ antiporter NhaA from Escherichia coli: an electrophysiological study, J. Biol. Chem. 286 (2011) 23570–23581.
[70] E. Padan, S. Schuldiner, Bacterial Na^+/H^+ antiporters—molecular biology, Biochemistry and Physiology, in: W.N. Konnings, H.R. Kaback, J.S. Lolkema (Eds.), Handbook of Biological Physics, Elsevier Science B. V., 1996
[71] P.A. Ottow EA, M. Brosché, J. Kangasjärvi, P. Dibrov, C. Zörb, T. Teichmann, Molecular characterization of PeNhaD1: the first member of the NhaD Na+/H+ antiporter family of plant origin, Plant Mol. Biol. 58 (2005) 75–88.
[72] J. Dzioba-Winogrodzki, O. Winogrodzki, T.A. Krulwich, M.A. Boin, C.C. Hase, P. Dibrov, The Vibrio cholerae Mrp system: cation/proton antiport properties and enhancement of bile salt resistance in a heterologous host, J. Mol. Microbiol. Biotechnol. 16 (2009) 176–186.
[73] T.H. Swartz, M. Ito, T. Ohira, S. Natsui, D.B. Hicks, T.A. Krulwich, Catalytic properties of Staphylococcus aureus and Bacillus members of the secondary cation/proton antiporter-3 (Mrp) family are revealed by an optimized assay in an Escherichia coli host, J. Bacteriol. 189 (2007) 3081–3090.
[74] L. Guan, H.R. Kaback, Site-directed alkylation of cysteine to test solvent accessibility of membrane proteins, Nat. Protoc. 2 (2007) 2012–2017.
[75] M.H. Akabas, C. Kaufmann, P. Archdeacon, A. Karlin, Identification of acetylcholine receptor channel-lining residues in the entire M2 segment of the alpha subunit, Neuron 13 (1994) 919–927.
[76] M.H. Akabas, D.A. Stauffer, M. Xu, A. Karlin, Acetylcholine receptor channel structure probed in cysteine-substitution mutants, Science 258 (1992) 307–310.
[77] Y. Olami, A. Rimon, Y. Gerchman, A. Rothman, E. Padan, Histidine 225, a residue of the NhaA-Na^+/H^+ antiporter of *Escherichia coli* is exposed and faces the cell exterior, J. Biol. Chem. 272 (1997) 1761–1768.
[78] K. Herz, A. Rimon, E. Olkhova, L. Kozachkov, E. Padan, Transmembrane segment II of NhaA Na+/H+ antiporter lines the cation passage, and Asp65 is critical for pH activation of the antiporter, J. Biol. Chem., 285 2211–2220.
[79] M. Diab, A. Rimon, T. Tzubery, E. Padan, Helix VIII of NhaA Na(+)/H(+) antiporter participates in the periplasmic cation passage and pH regulation of the antiporter, J. Mol. Biol. 413 (2011) 604–614.
[80] T. Tzubery, A. Rimon, E. Padan, Structure-based functional study reveals multiple roles of transmembrane segment IX and loop VIII–IX in NhaA Na+/H + antiporter of Escherichia coli at physiological pH, J. Biol. Chem. 283 (2008) 15975–15987.
[81] T. Tzubery, A. Rimon, E. Padan, Mutation E252C increases drastically the K_m value for Na^+ and causes an alkaline shift of the pH dependence of NhaA Na^+/H^+ antiporter of *Escherichia coli*, J. Biol. Chem. 279 (2004) 3265–3272.
[82] L. Galili, A. Rothman, L. Kozachkov, A. Rimon, E. Padan, Transmembrane domain IV is involved in ion transport activity and pH regulation of the NhaA-Na^+/H^+ antiporter of *Escherichia coli*, Biochemistry 41 (2002) 609–617.
[83] L. Galili, K. Herz, O. Dym, E. Padan, Unraveling functional and structural interactions between transmembrane domains IV and XI of NhaA Na+/H+ antiporter of Escherichia coli, J. Biol. Chem. 279 (2004) 23104–23113.
[84] H. Inoue, T. Noumi, T. Tsuchiya, H. Kanazawa, Essential aspartic acid residues, Asp-133, Asp-163 and Asp-164, in the transmembrane helices of a Na+/H+ antiporter (NhaA) from Escherichia coli, FEBS Lett. 363 (1995) 264–268.
[85] T. Noumi, H. Inoue, T. Sakurai, T. Tsuchiya, H. Kanazawa, Identification and characterization of functional residues in a Na+/H+ antiporter (NhaA) from Escherichia coli by random mutagenesis, J. Biochem. (Tokyo) 121 (1997) 661–670.
[86] Y. Nie, I. Smirnova, V. Kasho, H.R. Kaback, Energetics of ligand-induced conformational flexibility in the lactose permease of Escherichia coli, J. Biol. Chem. 281 (2006) 35779–35784.
[87] M.J. Harms, J.L. Schlessman, G.R. Sue, B. Garcia-Moreno, Arginine residues at internal positions in a protein are always charged, Proc. Natl. Acad. Sci. U. S. A. 108 (2011) 18954–18959.
[88] A. Picollo, Y. Xu, N. Johner, S. Berneche, A. Accardi, Synergistic substrate binding determines the stoichiometry of transport of a prokaryotic H(+)/Cl(−) exchanger, Nat. Struct. Mol. Biol. 19 (2012) 525–531(S521).
[89] Y. Gerchman, Y. Olami, A. Rimon, D. Taglicht, S. Schuldiner, E. Padan, Histidine-226 is part of the pH sensor of NhaA, a Na^+/H^+ antiporter in *Escherichia coli*, Proc. Natl. Acad. Sci. U. S. A. 90 (1993) 1212–1216.
[90] E. Padan, D. Zilberstein, H. Rottenberg, Eur. J. Biochem. 63 (1976) 533–541.
[91] L.M. Veenhoff, E.H. Heuberger, B. Poolman, Quaternary structure and function of transport proteins, Trends Biochem. Sci. 27 (2002) 242–249.
[92] A. Rimon, T. Tzubery, E. Padan, Monomers of nhaa NA+/H+ antiporter of Escherichia coli are fully functional yet dimers are beneficial under extreme stress conditions at alkaline ph in the presence of NA + or LI+, J. Biol. Chem. 282 (2007) 26810–26821.
[93] E. Screpanti, E. Padan, A. Rimon, H. Michel, C. Hunte, Crucial steps in the structure determination of the Na+/H+ antiporter NhaA in its native conformation, J. Mol. Biol. 362 (2006) 192–202.
[94] T. Mager, M. Braner, D. Alkoby, A. Rimon, E. Padan, K. Fendler, Differential effects of mutations on the transport properties of NhaA from Escherichia coli, J. Biol. Chem. 288 (2013) 24666–24675.
[95] K.A. Williams, Three-dimensional structure of the ion-coupled transport protein NhaA, Nature 403 (2000) 112–115.
[96] X. Jiang, A.J. Driessen, B.L. Ferringa, H.R. Kaback, The periplasmic cavity of LacY mutant Cys154-Gly: how open is open? Biochemistry 52 (2013) 6568–6574.
[97] D. Drew, M. Lerch, E. Kunji, D.J. Slotboom, J.W. de Gier, Optimization of membrane protein overexpression and purification using GFP fusions, Nat. Methods 3 (2006) 303–313.
[98] Y. Sonoda, S. Newstead, N.J. Hu, Y. Alguel, E. Nji, K. Beis, S. Yashiro, C. Lee, J. Leung, A.D. Cameron, B. Byrne, S. Iwata, D. Drew, Benchmarking membrane protein detergent stability for improving throughput of high-resolution X-ray structures, Structure 19 (2011) 17–25.
[99] T. Kawate, E. Gouaux, Fluorescence-detection size-exclusion chromatography for precrystallization screening of integral membrane proteins, Structure 14 (2006) 673–681.
[100] D.M. Rosenbaum, V. Cherezov, M.A. Hanson, S.G. Rasmussen, F.S. Thian, T.S. Kobilka, H.J. Choi, X.J. Yao, W.I. Weis, R.C. Stevens, B.K. Kobilka, GPCR engineering yields high-resolution structural insights into beta2-adrenergic receptor function, Science 318 (2007) 1266–1273.
[101] R. Ujwal, D. Cascio, J.P. Colletier, S. Faham, J. Zhang, L. Toro, P. Ping, J. Abramson, The crystal structure of mouse VDAC1 at 2.3 A resolution reveals mechanistic insights into metabolite gating, Proc. Natl. Acad. Sci. U. S. A. 105 (2008) 17742–17747.
[102] M. Caffrey, V. Cherezov, Crystallizing membrane proteins using lipidic mesophases, Nat. Protoc. 4 (2009) 706–731.
[103] J. Payandeh, T.M. Gamal El-Din, T. Scheuer, N. Zheng, W.A. Catterall, Crystal structure of a voltage-gated sodium channel in two potentially inactivated states, Nature 486 (2012) 135–139.
[104] U. Pieper, A. Schlessinger, E. Kloppmann, G.A. Chang, J.J. Chou, M.E. Dumont, B.G. Fox, P. Fromme, W.A. Hendrickson, M.G. Malkowski, D.C. Rees, D.L. Stokes, M.H. Stowell, M.C. Wiener, B. Rost, R.M. Stroud, R.C. Stevens, A. Sali, Coordinating the impact of structural genomics on the human alpha-helical transmembrane proteome, Nat. Struct. Mol. Biol. 20 (2013) 135–138.
[105] S.K. Singh, A. Yamashita, E. Gouaux, Antidepressant binding site in a bacterial homologue of neurotransmitter transporters, Nature 448 (2007) 952–956.
[106] S.K. Singh, C.L. Piscitelli, A. Yamashita, E. Gouaux, A competitive inhibitor traps LeuT in an open-to-out conformation, Science 322 (2008) 1655–1661.
[107] C. Ostermeier, S. Iwata, B. Ludwig, H. Michel, Fv fragment-mediated crystallization of the membrane protein bacterial cytochrome c oxidase, Nat. Struct. Biol. 2 (1995) 842–846.
[108] E. Padan, M. Venturi, H. Michel, C. Hunte, Production and characterization of monoclonal antibodies directed against native epitopes of NhaA, the Na+/H+ antiporter of Escherichia coli, FEBS Lett. 441 (1998) 53–58.
[109] M. Venturi, A. Rimon, Y. Gerchman, C. Hunte, E. Padan, H. Michel, The monoclonal antibody 1F6 identifies a pH-dependent conformational change in the hydrophilic NH_2 terminus of NhaA Na^+/H^+ antiporter of *Escherichia coli*, J. Biol. Chem. 275 (2000) 4734–4742.
[110] M.J. Serrano-Vega, F. Magnani, Y. Shibata, C.G. Tate, Conformational thermostabilization of the beta1-adrenergic receptor in a detergent-resistant form, Proc. Natl. Acad. Sci. U. S. A. 105 (2008) 877–882.
[111] A.I. Alexandrov, M. Mileni, E.Y. Chien, M.A. Hanson, R.C. Stevens, Microscale fluorescent thermal stability assay for membrane proteins, Structure 16 (2008) 351–359.
[112] R.M. Bill, P.J. Henderson, S. Iwata, E.R. Kunji, H. Michel, R. Neutze, S. Newstead, B. Poolman, C.G. Tate, H. Vogel, Overcoming barriers to membrane protein structure determination, Nat. Biotechnol. 29 (2011) 335–340.
[113] K.Y. Chung, S.G. Rasmussen, T. Liu, S. Li, B.T. DeVree, P.S. Chae, D. Calinski, B.K. Kobilka, V.L. Woods Jr., R.K. Sunahara, Conformational changes in the G protein Gs induced by the beta2 adrenergic receptor, Nature 477 (2011) 611–615.
[114] E. Olkhova, L. Kozachkov, E. Padan, H. Michel, Combined computational and biochemical study reveals the importance of electrostatic interactions between the "pH sensor" and the cation binding site of the sodium/proton antiporter NhaA of Escherichia coli, Proteins 76 (2009) 548–559.
[115] E. Olkhova, C. Hunte, E. Screpanti, E. Padan, H. Michel, Multiconformation continuum electrostatics analysis of the NhaA Na+/H+ antiporter of Escherichia coli with functional implications, Proc. Natl. Acad. Sci. U. S. A. 103 (2006) 2629–2634.
[116] E. Olkhova, E. Padan, H. Michel, The influence of protonation states on the dynamics of the NhaA antiporter from Escherichia coli, Biophys. J. 92 (2007) 3784–3791.

[117] Y. Gerchman, A. Rimon, E. Padan, A pH-dependent conformational change of NhaA Na^+/H^+ antiporter of *Escherichia coli* involves loop VIII–IX, plays a role in the pH response of the protein, and is maintained by the pure protein in dodecyl maltoside, J. Biol. Chem. 274 (1999) 24617–24624.
[118] S. Radestock, L.R. Forrest, The alternating-access mechanism of MFS transporters arises from inverted-topology repeats, J. Mol. Biol. 407 (2011) 698–715.
[119] A. Rothman, Y. Gerchman, E. Padan, S. Schuldiner, Probing the conformation of NhaA, a Na+/H+ antiporter from Escherichia coli, with trypsin, Biochemistry 36 (1997) 14572–14576.
[120] A. Rimon, C. Hunte, H. Michel, E. Padan, Epitope mapping of conformational monoclonal antibodies specific to NhaA Na+/H+ antiporter: structural and functional implications, J. Mol. Biol. 379 (2008) 471–481.
[121] L. Kozachkov, E. Padan, Site-directed tryptophan fluorescence reveals two essential conformational changes in the Na+/H+ antiporter NhaA, Proc. Natl. Acad. Sci. U. S. A. 108 (2011) 15769–15774.
[122] Y. Huang, M.J. Lemieux, J. Song, M. Auer, D.N. Wang, Structure and mechanism of the glycerol-3-phosphate transporter from Escherichia coli, Science 301 (2003) 616–620.
[123] M. Schushan, A. Bhattacharjee, N. Ben-Tal, S. Lutsenko, A structural model of the copper ATPase ATP7B to facilitate analysis of Wilson disease-causing mutations and studies of the transport mechanism, Metallomics 4 (2012) 669–678.
[124] P. Schulz, J.J. Garcia-Celma, K. Fendler, SSM-based electrophysiology, Methods 46 (2008) 97–103.
[125] I. Smirnova, V. Kasho, J. Sugihara, H.R. Kaback, Probing of the rates of alternating access in LacY with Trp fluorescence, Proc. Natl. Acad. Sci. U. S. A. 106 (2009) 21561–21566.
[126] I. Smirnova, V. Kasho, J. Sugihara, J.L. Vazquez-Ibar, H.R. Kaback, Role of protons in sugar binding to LacY, Proc. Natl. Acad. Sci. U. S. A. 109 (2012) 16835–16840.
[127] Y. Zhao, D. Terry, L. Shi, H. Weinstein, S.C. Blanchard, J.A. Javitch, Single-molecule dynamics of gating in a neurotransmitter transporter homologue, Nature 465 (2010) 188–193.
[128] Y. Zhao, D.S. Terry, L. Shi, M. Quick, H. Weinstein, S.C. Blanchard, J.A. Javitch, Substrate-modulated gating dynamics in a Na+-coupled neurotransmitter transporter homologue, Nature 474 (2011) 109–113.
[129] P. Dibrov, D. Taglicht, Mechanismof Na/H exchange by Escherichia coli NhaA in reconstituted proteoliposomes, FEBS Lett. 336 (1993) 525–529.